frontiers | Frontiers in Ecology and Evolution

ORIGINAL RESEARCH
published: 13 April 2022
doi: 10.3389/fevo.2022.818417

Late Pleistocene–Holocene Palaeoenvironmental Evolution of the Makgadikgadi Basin, Central Kalahari, Botswana: New Evidence From Shallow Sediments and Ostracod Fauna

Fulvio Franchi[1], Barbara Cavalazzi[2,3], Mary Evans[4], Sevasti Filippidou[5], Ruaraidh Mackay[2], Paolo Malaspina[2], Goitse Mosekiemang[1], Alex Price[5] and Veronica Rossi[2]*

[1] Department of Earth and Environmental Science, Botswana International University of Science and Technology, Palapye, Botswana, [2] Department of Biological, Geological and Environmental Sciences (BiGeA), Università di Bologna, Bologna, Italy, [3] Department of Geology, University of Johannesburg, Johannesburg, South Africa, [4] School of Geography, Archaeology and Environmental Studies, University of the Witwatersrand, Johannesburg, South Africa, [5] School of Environment, Earth and Ecosystem Sciences, The Open University, Milton Keynes, United Kingdom

OPEN ACCESS

Edited by:
Laura Parducci,
Sapienza University of Rome, Italy

Reviewed by:
Zhongping Lai,
Shantou University, China
Ilaria Mazzini,
National Research Council (CNR), Italy

***Correspondence:**
Fulvio Franchi
franchif@biust.ac.bw

Specialty section:
This article was submitted to Paleoecology, a section of the journal Frontiers in Ecology and Evolution

Received: *19 November 2021*
Accepted: *10 March 2022*
Published: *13 April 2022*

Citation:
Franchi F, Cavalazzi B, Evans M, Filippidou S, Mackay R, Malaspina P, Mosekiemang G, Price A and Rossi V (2022) Late Pleistocene–Holocene Palaeoenvironmental Evolution of the Makgadikgadi Basin, Central Kalahari, Botswana: New Evidence From Shallow Sediments and Ostracod Fauna. Front. Ecol. Evol. 10:818417. doi: 10.3389/fevo.2022.818417

The Makgadikgadi Basin in Botswana hosts a system of salt lakes, which developed from the Upper Pleistocene onward due to the gradual shrinking of the giant Lake Palaeo-Makgadikgadi. Stratigraphic and palaeoclimatic studies of this area are difficult due to the influence of several factors, such as a complex history of regional tectonic activities, as well as climatic changes coupled with dryland diagenetic processes. This lake, in the central Kalahari, is the key to understanding the climatic variability in the southern part of Africa in the Quaternary and has played an important role in the evolution of numerous taxa, including our own. In this study, detailed sedimentological analyses (grain size and major elements distribution) of shallow sediments from the Makgadikgadi Pans were combined with the first comprehensive study of the encountered ostracod fauna to establish trends in the environmental changes in the area from the late Quaternary. Ostracod fossil assemblages from the cores of the Makgadikgadi Pans are dominated by the *Limnocythere* ssp., an opportunistic taxa commonly colonizing the littoral areas of shallow evaporative, ephemeral lakes, together with the subordinate occurrences of *Sarcypridopsis ochracea*, *Sclerocypris* cf. *bicornis, Candonopsis* spp., and *Ilyocypris* spp. The sediments from the pans show fluctuations in the Cl/K and Ca/Cl ratios, often in phase with the relative abundance of *Limnocythere* suggesting a cyclicity induced by changes of salinity and alkalinity in the water. This multi-proxy study of the cores collected from the pans suggests a Late Pleistocene shallow, playa lake environment with strongly alkaline water, interrupted by a prolonged drought with sustained aeolian conditions between ∼16 and 2 ka BP. Increasing

diversity of ostracod fauna in the top 20–30 cm of the cores indicates that a temporary shift toward higher humidity occurred around 2–1.5 ka BP and lasted through the Medieval Warm Period. This humid period was followed by an overall desiccation trend that started with the Little Ice Age and continues until the present day.

Keywords: Kalahari, playa lake, evaporites, ostracods, late Quaternary

INTRODUCTION

The Makgadikgadi Basin (MB) in central Botswana (**Figure 1A**) is the relict area of a mega-lake system, known as Lake Palaeo-Makgadikgadi (LPM) (Grey and Cooke, 1977; Cooke and Verstappen, 1984; Thomas and Shaw, 1991; Eckardt et al., 2008; Burrough et al., 2009a,b; Riedel et al., 2012, 2014; McFarlane and Long, 2015; Schmidt et al., 2017). Today the MB hosts the world's largest salt pans complex (e.g., Podgorski et al., 2013), including the Sua and the Ntwetwe Pans (**Figure 2**), and it represents a key area to investigate the Late Pleistocene–Holocene environmental changes occurring in southern Africa and their possible connection with climate variability (Burrough and Thomas, 2013). However, the age uncertainty of the LPM sediments and the complex depositional dynamics of (ephemeral) saline lacustrine systems fuelled a decade-long controversy regarding the evolution of the central and northern Kalahari (Schmidt et al., 2017).

Moreover, being hydrologically linked with the Cubango–Okavango River Basin systems as part of the Makgadikgadi–Okavango–Zambezi Basin (MOZB; Ringrose et al., 2005; Huntsman-Mapila et al., 2006), the MB has played a pivotal role in the distribution of surface and underground water reserves in an otherwise arid to semi-arid climate. The MB has been the center of important species radiations (Joyce et al., 2005) and is considered a potential cradle of modern human beings as it provided a suitable environment for settlements as far back as 200 ka (Chan et al., 2019).

Seven highstand phases of Late Pleistocene–Holocene age were identified based on the altitudes of the palaeo-shorelines identified across the LPM. Three highstand phases were dated between 130 and 60 ka by luminescence techniques applied on shoreline sands; the other four took place over the last 40 ka: 38.7 ± 1.8 ka, 26.8 ± 1.2 ka, 17.1 ± 1.6 ka, and 8.5 ± 0.2 ka (Burrough et al., 2009a; Schmidt et al., 2017). On the contrary, a few studies have analyzed the subsurface record of the MB so far (Riedel et al., 2014; Schmidt et al., 2017; Richards et al., 2021) concluding that a spatial correlation of sediments and faunal associations across the basin is still lacking in the literature.

This work is focused on the reconstruction of the evolution trends of the LPM between the penultimate highstand phase (17.1 ± 1.6 ka; Burrough et al., 2009a; Schmidt et al., 2017) and the current condition of the ephemeral lake (playa). Shallow cores, collected from seven sites belonging to both Sua and Ntwetwe pans (**Figures 1B**, **2**), were mainly studied in terms of grain size, major elements distribution, and ostracod fauna. Selected samples from a sampling site in the Sua Pan were dated using the Optical Stimulated Luminescence (OSL) technique and results were compared with existing radiometric ages from literature. Subsurface bio-sedimentary data were then combined for the first time along with cores stratigraphy, with the specific aim to furnish new insights on the palaeoenvironmental dynamics of the Sua and Ntwetwe Pans focusing on the Pleistocene–Holocene transition onwards.

GEOLOGICAL SETTING

The bedrock of the MB consists of Carboniferous to Early Jurassic volcano-sedimentary units belonging to the Karoo Supergroup (**Figure 2**; see details in Modie and Le Hérrissé, 2009; Bordy, 2020; Franchi et al., 2021). The MB is crossed by an ESE–WNW trending doleritic dyke swarm of the Karoo large igneous province (∼187 Ma old; Elburg and Goldberg, 2000; **Figure 2**). The Karoo Supergroup units are covered by an estimated 50–300 m-thick succession of aeolian sands, lacustrine and fluvial deposits, and duricrusts of pedogenic origin of the Kalahari Group (Thomas and Shaw, 1991; Haddon and McCarthy, 2005).

The LPM system developed within the ∼120,000 km^2 MOZB as part of the south-western branch of the East African Rift System (EARS) (Riedel et al., 2014; Schmidt et al., 2017). Its evolution is controlled by NE–SW faults closely related to the EARS propagation toward SW (Modisi et al., 2000; Kinabo et al., 2007). The oldest dated LPM strandlines yielded OSL ages of 288 ± 25 ka (Burrough et al., 2009a); however, the presence of Early Stone Age tools in the basin suggested that a precursor of the LPM was already present ∼500 ka BP (McFarlane and Eckard, 2006).

Some authors attributed the formation of the early lake system in the central Kalahari Basin to the activation (uplift) of the Chobe Fault during the Early Pleistocene (Moore et al., 2012). This early stage of evolution culminated in the formation of the palaeo mega-lake Deception, a precursor of the LPM (Moore et al., 2012). In the Early to Middle Pleistocene, the uplift of the Congo–Zambezi watershed reduced the hydrological input into the basin. Therefore, the LPM outlined by the shoreline at ∼945 m a.s.l. was formed (Thomas and Shaw, 1991; Moore et al., 2012). This phase was followed by a further, progressive contraction of the lake shoreline to ∼936, 920, and 912 m a.s.l (Thomas and Shaw, 1991; Moore et al., 2012). During the Middle to Late Pleistocene, the activation of the Okavango graben in the north-west of the Makgadikgadi Basin led to the formation of the Okavango Delta and the Makgadikgadi Pans (Burrough et al., 2009b; Moore et al., 2012). At ∼46 ky BP the main inflow in the basin was from the palaeo-Boteti and palaeo-Nata rivers and the level of the lake was at ∼912 m a.s.l (Riedel et al., 2014).

During the Last Glacial Maximum, when the lake level rose to 936 m a.s.l (Riedel et al., 2014), the Okwa River (**Figure 1A**) was

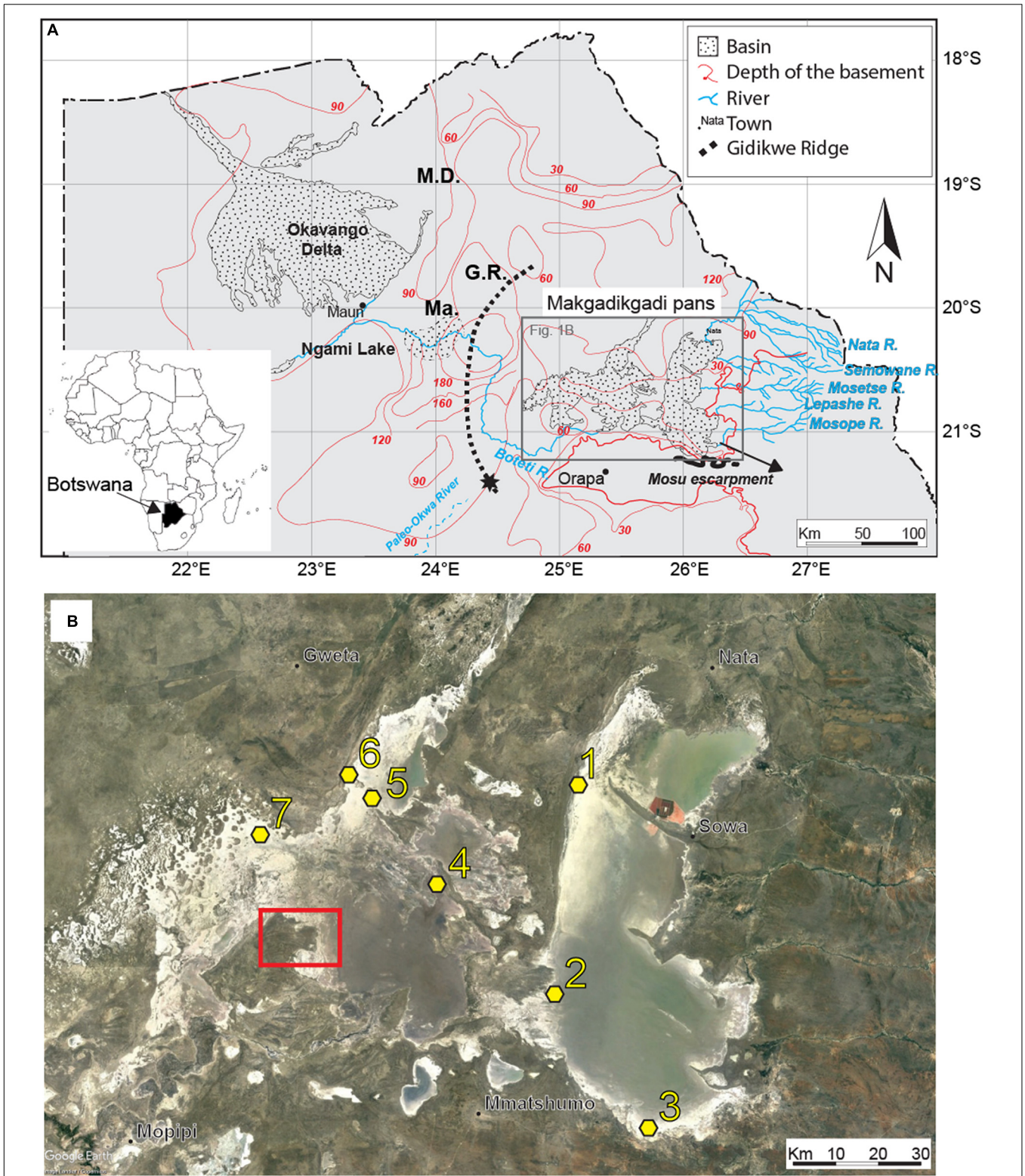

FIGURE 1 | (A) Schematic view of the main basins in northern Botswana, showing the main affluent to the Makgadikgadi Pans and relevant geomorphic features. The star indicates the terminal Okwa Valley (Riedel et al., 2012). Ma, Makalamabedi Basin; G.R., Gidikwe ridge; M.D., Mababe Depression. **(B)** Satellite image of the Makgadikgadi Pans showing the sampling sites (yellow). 1, Sua Pan Nord core; 2, Kubu Island core, near the core presented in Riedel et al. (2012, 2014); 3, Mosu core; 4, NT mounds cores; 5, LM core; 6, NT shore core; 7, RM mound cores. Source Google Earth, Image Landsat/Copernicus, US Department of State Geographer, 2021. Red square outlines the fan delta described in Franchi et al. (2020), **Figure 4** therein.

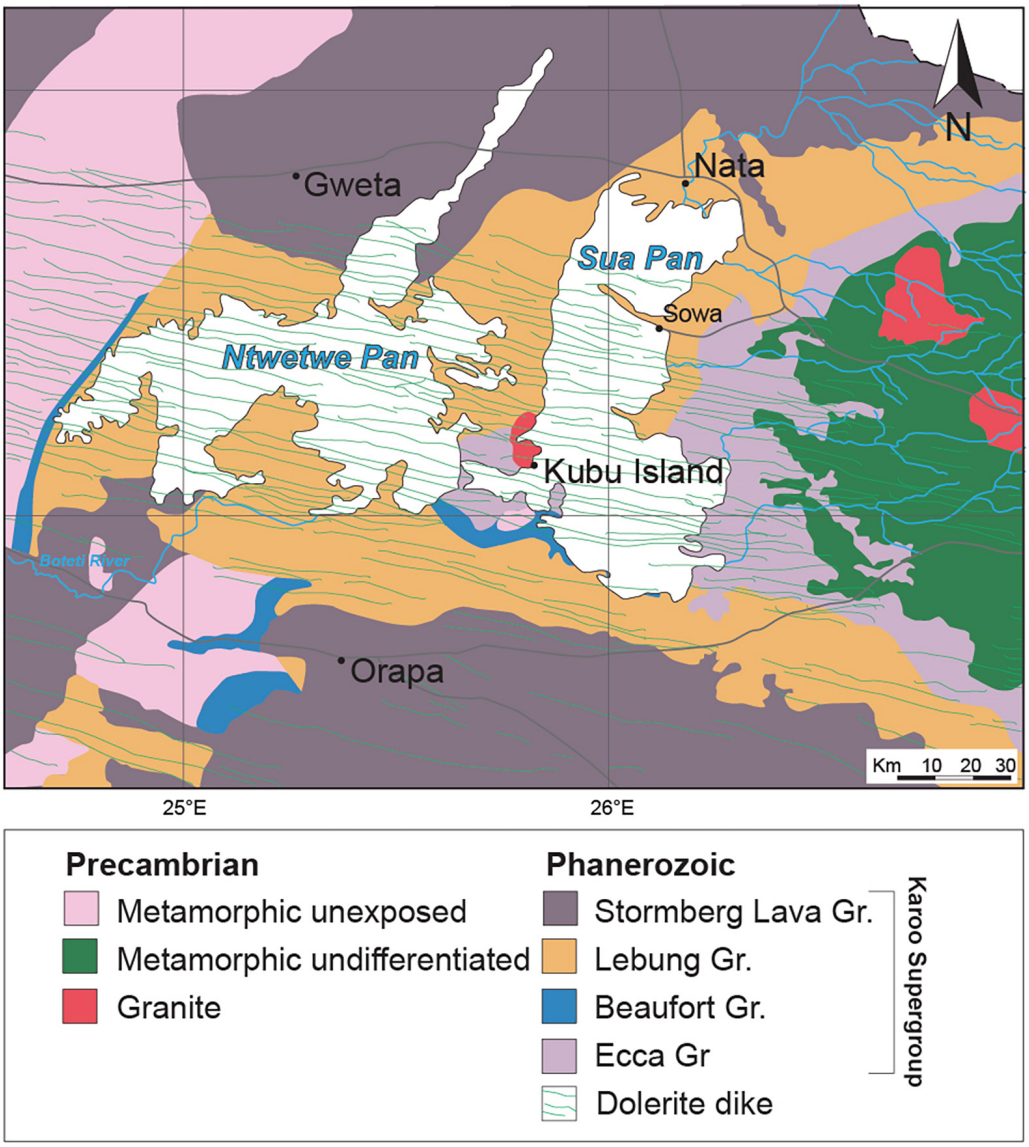

FIGURE 2 | Schematic geological map of the Makgadikgadi Basin. Modified from Key (1997).

one of the main tributaries of the LPM (Shaw et al., 1992; Nash et al., 1994; Nash and McLaren, 2003). Then, during the mid-Holocene the level of the lake dropped to 920 m a.s.l. and then to ∼908 m a.s.l. over the last millennium (Riedel et al., 2014).

Today, the MB receives seasonal surface water from local rainfall and is principally fed by ephemeral rivers flowing from the east and north-east, and seasonally by the Boteti River in the south-west (**Figure 1A**). The climate of the MB is arid to semi-arid, receiving relatively low mean annual rainfall (∼300 mm yr^{-1}) with precipitation limited to the summer season (Burrough et al., 2009a). During the winter dry season (between April and October), the dominant processes are wind erosion and calcretization under playa conditions (Riedel et al., 2012). Water table fluctuations, between the wet and dry seasons, and the seasonal flooding contribute to the deposition of an ephemeral crust of evaporites and clays on the pan floor (Eckardt et al., 2008; Ringrose et al., 2009), leading to the development of consolidated surfaces (pavements). Moreover, the shallow subsurface of the pan is characterized by sub-cropping duricrusts (e.g., Nash et al., 1994).

MATERIALS AND METHODS

Field Work, Sedimentological, and Geochemical Analyses

Several field campaigns were conducted between September 2017 and January 2020 across the Makgadikgadi Pans. These activities were focused in the western part of the Sua Pan and along the north-western shores of the Ntwetwe Pan (**Figure 2**). The

western Sua Pan was selected as it is the most accessible site with active precipitation of evaporites and is cyclically inundated (McCulloch et al., 2008). A sampling site near Kubu Island (Point 2 in **Figure 1B**) was also chosen to allow comparisons with radiocarbon ages from a core described by Riedel et al. (2012, 2014). The north-western shores of the Ntwetwe Pan were selected for being affected by active coastline erosion during the evolution of the pan and for the presence of well-known morphologies such as barchan dunes, layered mounds, and strandlines described in the literature (Cooke, 1980; Burrough and Thomas, 2013; Franchi et al., 2020; Richards et al., 2021). Seven coring sites (**Figure 1B** and **Table 1**) were sampled using a manual percussion corer with a 20 cm stainless steel barrel, 5 cm in diameter, and an internal PVC liner, 15 cm in length, to acquire a total of nine cores up to 380 cm long (**Table 1**). Five cores were collected from mounds in the Ntwetwe Pan (RM3, RM5, NT2, NT3, and LM) and one from the pan strandline (NT shore) (**Table 1**). Three cores were collected from the Sua Pan floor (∼903 m a.s.l.) along a transect approximately S–N (**Table 1**). The uppermost 60–80 cm were often composed of fine loose, poorly cohesive sediments that were destructively extracted with an Auger corer every 10 cm. The lowermost 5 cm of cored sediment was retained within the nose of the stainless steel barrel and stored separately. All the cores were described and sub-sampled at 2 cm intervals (when possible) for laboratory analyses.

All sedimentological and geochemical analyses were performed at the Botswana International University of Science and Technology—BIUST (Botswana). The grain size distribution of sediment samples was obtained using a Malvern Mastersizer 3,000 laser diffraction particle size analyzer. Organic matter content was determined using the Loss on Ignition (LOI) method whereby the samples were dried at 60°C for 24 h and subsequently ignited for 2 h in a funnel furnace at 550°C (**Table 2**).

The three cores obtained from the Sua Pan were investigated for their geochemical composition since they represent sites with active evaporite and clay deposition. Major and trace elements distributions were obtained with a Bruker DELTA Premium Handheld X-ray Fluorescence (XRF) spectrometer (**Table 2**). A detailed description of the vertical variation of selected elements in the cores from the Sua Pan in relationship with sedimentological features and textures is provided in **Table 3**.

Ostracod Analysis

A total of 65 samples were collected along the length of the cores in order to characterize all the encountered lithological units in terms of ostracod content, focusing on the silty-muddy intervals where the presence of other fossil remains (mainly gastropods shells or fragments) was suggestive of an autochthonous fauna. The North Sua Pan core was not analyzed as it shows a stratigraphy almost identical to that recovered at the Kubu Island site (**Figure 2**).

All samples were prepared at BIUST following a standard procedure (e.g., Amorosi et al., 2014). At least 100 well-preserved valves with morphological features sufficiently developed to allow taxonomic classification was picked and counted (carapaces were considered as two valves), when possible. In the same sediment fraction, heavily recrystallized ostracods were also extracted and analyzed separately. Taxonomic identification of ostracods and autoecological information were based on Meisch (2000) and several reference papers dealing with modern and late Quaternary ostracod fauna from the Makgadikgadi Pans and African inland lakes and wetlands (e.g., Cohen et al., 1983; Martens et al., 1996; Holmes et al., 1998; McCulloch et al., 2008; Park and Cohen, 2011; Bristow et al., 2018; see also **Table 4**).

A selection of ostracod shells was analyzed for morphology and chemical composition using a Jeol JSM-5200 Scanning Electron Microscope (SEM) equipped with an Electron Dispersive Spectrometer (EDS) IXRF Iridium at the BiGeA Department, University of Bologna. EDS analysis was undertaken on different areas of the selected valves in order to evaluate data consistency.

Optical Stimulated Luminescence Dating

Two samples from the Kubu Island core (**Table 5**) were dated using the OSL dating technique at the Luminescence Dating Laboratory of the University of the Witwatersrand (South Africa). The samples were left intact within their PVC liners and sealed carefully to ensure no exposure to sunlight and were prepared under red, safe-light conditions. Quartz grains with a size range

TABLE 1 | List and coordinates of studied localities, length of the cores, and elevation.

Location	Core name	Lat	Long	Core Length (cm)	Altitude (m a.s.l.)	
					Pan Floor	Core top
Sua	Kubu Island	–20,89717	25.8289	80	903.0	–
	Southern Sua Pan-Mosu	–21.18837	26.04583	190	903.0	–
	Northern Sua Pan	–20.45827	25.88975	103	903.0	–
Ntwetwe	NT shore	–20.44236	25.37123	260	913.4	916.4
	Mounds					
	RM5	–20.56294	25.13959	390	913.4	918.0
	RM3	–20.55422	25.16474	310	916.3	920.2
	NT3	–20.47986	25.40849	195	915.0	916.4
	NT2	–20.48148	25.40825	135	915.0	916.9
	LM	–20.65400	25.57056	195	918.2	919.4

TABLE 2 | Chemical composition (XRF) and organic matter content (LOI) of the sediments from the Sua Pan.

Depth	S	Cl	K	Ca	Ti	V	Mn	Fe	Zn	Rb	Sr	Zr	Nb	Ba	Th	LOI
Northern Sua Pan																
1.5	3,086	68,717	6,717	1,11,269	448	146	107	4,854	14.2	83.6	981	57	3.3	939	27	14.73
4.5	3,645	94,805	5,653	1,24,216	322	196	97	3,519	11.5	54.5	1,083	39.1	2.8	567	32	20.50
7.5	2,208	26,641	8,069	1,68,060	505	227	129	4,861	12.9	60.9	903	34.9	2.6	486	22	21.55
10.5	3,623	94,762	4,288	1,10,261	289	163	81	2,553	8.7	51.9	569	22.9	1.4	390	15	19.59
13.5	2,553	2,23,208	2,068	45,271	126	48	54	2,227	7.9	81.2	872	48.2	3.7	904	27	16.05
16.5	1,027	1,78,193	2,067	22,634	122	61	58	1,841	9	76.1	414	25.4	2.5	453	13	19.18
19.5	–	2,57,138	1,381	14,748	73	–	35	1,459	9.7	79	529	39.1	3.1	630	17	18.33
22.5	1,255	2,54,788	1,139	12,058	67	50	35	1,800	8.6	74.5	547	39.3	2.8	671	19	18.22
25.5	1,839	2,48,824	1,426	16,741	228	84	49	2,369	11.7	82.1	506	35.7	3	476	13	15.94
28.5	–	2,19,177	977	9,855	67	50	41	1,297	5.5	54	465	34	2.1	580	12	16.78
32	3,714	19,5580	2,758	15,515	151	86	57	2,654	12.8	87.2	281	21	2.2	316	6	16.48
35.5	3,042	88,131	7,419	1,08,667	465	126	113	5,269	15.9	89.1	922	54	3.8	899	29	20.15
38.5	2,988	1,59,878	4,323	63,615	338	129	74	3,378	14.8	91.7	804	40.8	3.2	674	27	17.02
42	3,284	1,85,880	3,468	24,385	217	95	64	2,756	10.8	83.2	457	33.4	2.3	545	14.4	15.32
45.5	1,871	1,59,942	1,581	6,311	92	121	35	952	5.4	56.8	267	28.4	1.9	739	10.3	18.42
48.5	1,655	1,88,760	2,426	20,371	131	48	59	2,405	10.4	80.9	506	32.5	1.8	614	16	18.82
52.5	1,788	54,105	5,370	63,602	306	133	90	3,118	9.5	54.1	408	18.4	1.6	276	–	19.13
55.5	1,901	42,204	5,082	65,479	305	134	83	3,104	10.9	49.8	460	26.9	2	311	10	16.25
59	935	26,646	4,937	78,524	242	177	89	2,975	7.2	47.6	563	27.4	1.8	392	6.3	19.40
63	–	10,245	4,462	55,107	510	82	83	2,607	8.3	16	159.6	41.1	1.1	370	6.1	19.52
66.5	7,056	1,81,697	2,448	48,031	201	90	57	2,637	11.9	70.7	835	61	3.1	1,058	28	20.63
70	4,226	99,311	3,740	1,06,329	136	141	64	1,801	6	60.1	1,039	51.9	3.5	1,467	31	20.57
73.5	2,407	1,56,948	2,723	67,954	142	117	62	2,310	9.9	72.5	928	40.7	3	1,062	21	20.06
77	2,807	1,70,484	2,732	19,515	170	51	59	2,786	11.6	88.3	583	45.5	3.9	688	10	18.89
81	3,258	1,08,675	5,475	70,252	4,044	166	99	3,865	13.1	39.9	959	56.8	1.4	1,307	23	17.98
85.5	1,957	41,483	5,417	1,32,526	306	229	95	3,147	10.2	51.3	979	66	2.7	1,490	23	19.62
90.5	1,471	24,241	5,348	1,93,342	471	248	105	2,953	9.4	26	1,696	132	3.5	2,666	42	13.61
Kubu Island																
1.5	1,211	12,556	10,043	3,89,412	1,687	320	151	3,848	13.4	34.2	788	29.4	2.7	608	16.2	17.45
4.5	1,447	27,311	10,172	2,21,918	735	208	151	4,667	14.9	50	646	28.6	2.3	452	13.5	16.86
7.5	–	13,507	9,525	2,72,484	558	244	134	5,269	13.6	56.4	1,027	43.2	2.8	1,085	27	15.51
10.5	977	15,825	10,862	2,33,169	616	216	159	5,949	18.9	71.1	863	43.4	3.1	836	22	17.59
13.5	1,566	15,158	10,133	2,96,976	509	254	165	3,552	13.3	43.5	561	21.2	2.1	376	9.9	14.88
17.5	–	20,231	4,826	1,32,268	314	120	99	3,034	8.9	40.3	599	22.7	1.5	493	14	–
21	925	33,376	9,230	2,01,567	628	178	154	3,796	11.3	43.5	452	20.2	1.7	249	9.3	17.30
23	1,102	20,091	8,204	2,04,366	479	169	133	4,410	12.6	56.6	601	28.1	2.6	394	13.5	18.24
25	–	–	–	–	–	–	–	–	–	–	–	–	–	–	–	15.49
27	1,030	26,175	9,126	1,89,419	511	200	169	4,274	12.2	47	538	23.9	1.7	315	11.1	13.43
29	1,064	25,728	9,076	1,46,132	591	160	156	4,055	12.1	37.3	524	21	1.5	250	9.8	12.47
31	865	16,610	8,750	1,53,102	818	206	180	6,926	16.7	62.1	801	85.4	3.5	911	23	16.00
33.5	944	21,336	9,369	1,12,827	619	173	182	7,834	21.7	67.2	736	72	3.2	869	23	12.24
37.5	–	14,862	8,016	87,004	601	123	155	7,956	18.3	60.5	864	85.6	2.6	809	26	–
44.5	–	15,999	14,477	1,67,832	921	154	188	9,577	22.1	85	852	72.5	3.2	401	20	12.74
47.5	–	9,825	13,948	1,99,488	1,155	138	195	9,575	22.3	85.1	1,027	80	4.6	532	29	14.51
50.5	734	10,160	14,558	1,43,648	935	144	234	10,876	25.9	85.7	833	69.3	4.1	529	28	12.37
53.5	–	25,626	10,656	1,00,663	1,262	163	212	8,926	17.6	68.1	548	66.4	2.8	389	10.6	14.44
57.5	–	13,852	9,429	1,08,088	712	106	146	6,612	16.6	55.8	549	35.6	2.1	211	12.7	–
61.5	1,007	37,640	10,215	1,31,675	688	144	167	8,489	18.6	74.5	853	54.7	3.5	536	22	9.84
64.5	–	–	–	–	–	–	–	–	–	–	–	–	–	–	–	8.81
67.5	–	28,383	10,233	70,174	649	114	186	9,020	23.5	88.2	503	37.3	2.9	251	14	12.72
70.5	–	16,183	13,629	64,454	841	117	237	11,490	24.7	103	428	39.8	2.9	222	14.3	9.51
73.5	–	–	–	–	–	–	–	–	–	–	–	–	–	–	–	5.71
77.5	–	14,772	12,675	87,649	724	120	166	8,774	20.2	65.2	386	25.7	1.6	300	10.3	–

(Continued)

TABLE 2 | (Continued)

Depth	S	Cl	K	Ca	Ti	V	Mn	Fe	Zn	Rb	Sr	Zr	Nb	Ba	Th	LOI
Southern Sua Pan—Mosu																
2.5	–	21,825	7,613	63,469	826	165	163	8,237	21.7	65.4	363	67.7	3.6	519	9.2	15.09
7.5	683	24,002	10,057	1,10,771	1,158	222	224	11,334	30.7	95	700	123	6.8	977	24	–
13	1,364	46,907	8,651	1,64,503	984	218	193	7,772	23	78.6	775	117	5.5	1,285	25	15.69
18	1,250	18,301	10,454	1,70,490	1,285	275	215	9,763	26.5	81.8	850	142	5.9	1,151	25	12.79
22.5	–	6,888	2,855	49,934	375	111	48	1,439	3.5	9.7	162.3	47.9	1	402	5.9	6.17
27.5	600	8,936	2,798	57,047	1,029	145	80	1,650	3.5	7.9	121.4	51.9	1	418	5.4	3.01
32	393	9,192	3,445	52,963	1,186	130	59	1,702		9.8	150.8	108.7	1.5	209	5.4	1.41
35.5	–	15,544	10,372	1,19,174	1,365	187	214	9,496	26.3	78.3	609	152	5.1	726	22	12.71
38.5	1,289	35,129	8,633	1,15,279	1,065	184	199	9,719	25.4	82.1	605	108	5.3	730	21	14.49
42	–	24,458	8,878	84,885	1,069	166	203	9,776	27.1	85.6	578	102.3	6	1,188	15	8.15
45.5	–	16,041	6,433	67,125	738	122	96	2,909	7.4	25.6	252	102.4	1.8	339	9.4	2.76
48.5	1,275	1,84,226	3,007	15,572	2,130	–	70	3,034	12.7	61.6	191	124.2	2.6	455	10	7.50
51.5	1,416	69,436	2,563	28,455	9,727	–	111	2,018	–	25.3	191	74	–	238	–	11.07
54.5	1,281	40,264	10,037	68,653	2,002	115	189	6,298	13.1	65.4	369	245	4.7	693	16.3	3.48
57.5	1,328	99,696	5,371	32,917	1,588	147	130	5,055	14.3	53.1	255	138	2.8	456	10	7.40
61.5	2,185	59,854	6,609	55,088	1,869	158	127	4,366	11.3	45.3	334	286	4.1	577	14	4.15
66	–	15,562	7,303	1,04,359	1,007	144	159	6,320	17.1	49.6	413	102.5	3.2	547	10.3	6.64
70	1,563	44,869	9,261	95,351	1,243	213	198	10,167	28.4	91.3	485	112.6	5.4	623	9.4	11.45
73.5	1,979	64,120	6,907	1,13,127	1,050	214	174	6,882	17.3	67.9	658	139	4.4	704	16	11.13
76.5	790	2,22,158	1,943	36,788	329	102	78	3,503	15.7	70.5	877	249	6.3	1,033	27	7.18
79.5	1,323	2,36,928	1,980	31,771	591	79	74	2,662	8.1	59.7	712	166	4.9	995	21	5.95
82.5	1,865	87,022	4,053	19,759	1,961	–	82	1,798	6	37	181	70.5	2.5	317	7	6.17
85	485	15,134	5,451	22,053	532	79	65	2,013	4.7	21.2	102.1	43.4	–	177	4.1	2.97
88	–	13,258	7,711	47,985	1,545	122	136	3,691	7.1	25.7	158.9	152.9	2.1	324	7.4	1.93
91.5	481	17,339	10,354	28,697	1,370	134	127	5,135	12.8	47.3	123.8	182	1.9	274	9.9	4.01
94.5	–	15,823	12,017	30,196	1,450	113	148	6,391	13.4	56.9	145.1	185	3.5	335	6.7	4.03
97	1,724	67,529	8,127	16,103	1,005	104	142	6,827	16.6	69	138	201	4.8	344	8.8	4.06
100	1,097	44,019	11,095	57,992	1,098	135	196	7,641	20.9	68.6	311	113	3.8	325	13.9	4.41
103.5	779	24,097	9,649	81,375	1,417	205	166	5,766	14.3	51.7	199	145.1	2.4	465	6.8	4.72
107	1,816	1,37,793	3,137	33,839	671	77	92	3,190	10.6	53.2	474	186	3.8	749	16	9.36
110.5	770	19,343	11,337	99,868	990	124	192	9,012	22.7	69.1	506	123	4.3	506	19	13.30
115	1,171	33,297	12,623	96,607	1,278	165	228	11,047	26.3	89.1	505	153	5	558	20	9.04
119.5	1,088	30,779	12,532	83,605	1,427	173	202	8,406	17.4	66.3	334	173	3.7	357	12.6	12.41
122.5	2,690	1,07,984	7,245	29,132	973	120	114	5,032	12.8	56.9	199	197	3.3	631	11.2	5.40
125.5	2,404	65,660	9,843	34,626	1,132	96	123	5,775	14.3	63.8	200	192	4.3	430	9.4	4.48
129.5	2,238	1,59,503	4,389	47,338	545	122	161	6,028	19.8	86.9	498	143	3.9	417	18.6	10.27
134	1,535	1,58,714	2,742	22,746	373	85	102	4,542	12.3	67.4	296	128	3.3	503	9.9	3.92
138.5	867	24,846	9,143	1,15,768	1,111	180	202	8,658	21	69.9	511	105.2	4.4	742	13.4	12.73
142.5	1,010	33,971	7,495	50,569	1,130	112	129	5,205	15.4	49.3	247	149	3.8	416	11.4	8.52
145.5	2,192	1,22,050	5,765	25,129	883	103	136	5,630	18	73.4	342	156	3	329	12.2	–
148.5	2,952	1,36,195	5,067	20,404	929	104	83	3,538	9.3	58.7	176	201	4.3	440	11.7	10.28
152.5	–	31,341	11,688	51,445	1,290	110	183	7,143	16.1	68.3	275	182	3.5	389	15	8.21
156.5	1,088	1,71,699	2,697	13,570	301	70	67	2,898	10	60.9	246	123	2.5	390	14	7.77
159.5	972	45,373	8,933	44,116	915	103	124	4,774	11.4	59.3	218	119.4	3.5	446	14.5	5.90
163.5	1,518	1,65,113	3,993	23,349	937	105	110	5,189	14.1	68.2	296	162.3	4	501	11.4	6.66
168	887	24,717	11,399	81,977	1,409	142	185	6,234	14.6	61.8	421	165	3.4	546	21	12.23
171	811	1,51,963	3,693	23,949	609	118	116	4,984	17	60.6	329	165	3.5	425	13.3	6.99
173	2,643	2,04,747	2,439	10,419	396	78	63	3,376	216	58.7	194	177.1	3	474	11.6	9.50
176	1,707	2,07,136	5,050	58,406	415	107	203	7,059	24.4	76.3	771	95	4.9	406	36	6.71
179	1,175	66,347	8,341	89,371	689	170	316	5,585	17.9	60.1	461	117	4.8	722	20.2	14.44
181	801	32,262	10,845	85,460	876	213	229	5,000	14.9	59	389	136.7	4.5	955	20.6	20.00

The location of the samples taken is tabulated in ***Table 1****.*

TABLE 3 | Schematic description of the cores from Sua Pan (see **Table 1** for location), including a summary of the geochemical composition and organic matter content (LOI).

	Depth (cm)	Description	LOI (%)	Geochemistry variations in the profile
Northern Sua Pan	0–10	Cream white to greenish compacted sandy silt with clumps of mud	20	High Ca, V, Mn, Fe, and S
	10–34		<20	Low Ca, V, Mn and Fe; high Rb
	34–38	Light colored (cream white), unconsolidated silt with clumps of darker mud	20	Peak of K, Ca, Mn, Fe, Zn, Sr, and Zr
	38–44	Light colored (cream white), consolidated silt with coarse sand and with clumps of darker mud	20	Low Ca, Mn, and Fe
	44–51	Dark green/grayish, consolidated silt with coarse sand and clumps of darker mud		
	51–65	Light colored (cream white), muddy sand. Gradual upper contact	20	Slight increase of Ca; peak of V
	65–68	Non-consolidated, sandy silt with clumps of mud some of which light in color toward the bottom of the layer. Clasts of quartz and fragments of shells	20	Low Ca, V and Mn; increasing Zn, Rb, Sr, and Zr
	68–72	Non-consolidated, sandy silt with clumps of mud some of which light in color toward the bottom of the layer. Clasts of quartz and fragments of shells	20	High Ca, V, Sr; Low Fe, Zn
	72–80	Grayish, consolidated silt with a sharp transition to overlaying unit	20	Peak of S; low Ca and V; increasing Fe, Zn, and Rb
	80–103	Grayish, sandy silt to fine sand with clumps of dark gray mud and grains of quartz. No stratigraphy was preserved	<10	Decreasing S; Ca, V, Mn, Fe, Zn, Sr, Zr, and Ba gradually increase downcore; the peak of Ti at 81 cm;
Kubu island	0–3	Fine grained, poorly sorted sand with calcite concretions	17	Low S; very high Ca, Ti and V
	3–7		17	High S; decrease of Ca, Ti and V
	7–14		>15	High Ca; peak Fe, Zn, Rb
	14–22	Light brown, poorly sorted, silty, fine grained sand		Decrease of Ca; Ti, V and Mn
	22–26		15–18	Steady decrease of Ca downcore
	26–30		13	Steady decrease of Ca downcore
	30–35	Dark brown, poorly sorted, silty, fine grained sand	16	Steady decrease of Ca downcore; low S; peak of Ti and V; sharp increase of Fe, Zn, Rb, Sr, Zr
	35–40		12	Steady decrease of Ca downcore; increase of all metals downcore
	40–51	Light brown to greenish, poorly sorted, fine grained sand with grains	15	Low S; Steady increase of Ca downcore; increase of Fe downcore; high metal contents
	51–55		14	Low Ca; peak of Ti; decrease of Fe, Mn and Zr
	55–70	Dark green, poorly sorted, silty, fine-grained sand with pebbles and cobbles of silcretes	<10	LOI increases downcore to 13%; low Ca and V; increasing Mn, Fe, Rb
	>70		<10	Lower Ca
Southern Sua Pan	0–5	Superficial layer is pale green, unconsolidated, sandy, and rich in whitish concretions	15	All metals are depleted
	5–20	Dark green with flat (flaky) concretions of dark green/black silcrete	15	High Ca; increase of all metal contents
	20–34	Loose sands with grains and pebbles of varying composition	<5	Decrease of all metal contents
	34–44	Dark green sandy layer with few sparse whitish concretions and mud chips; marked erosive base	15	High Ca; increase of all metal contents; LOI drops to 3%
	44–52	Dark green, consolidated (compacted) fine-grained sand with high organic content	15	Low Ca; peak of Ti and Rb; low Mn and Fe and other metals
	52–75	Dark green sandy mud with flat (flaky) dark green/black clasts of silcrete (cf. 5–16)	12	Slight increase of S; the gradual increase of Ca, V, Mn, Fe, Sr downcore;
	75–85	Light to dark green mud with sandy interlayers (cf. 50–64); Whitish sandy layer between 84 and 85. Erosive base (?)	7	The peak of Sr, Zr, and Rb
	85–90		<3	Low Ca; increase of V with depth; high Mn, Fe, Rb, Zr; low Sr and Ba
	90–104	Olive green compacted muddy/silty, sand with dark green nodules/mud chips	<5	High Mn, Fe, and Rb; low Sr and Ba
	104–110	Dark green silty, medium grained sand with clasts of white quartz, dark gray clay chips; basal sandy layer, sharp contact	12	Peak of Cl and very low K; low Ca and all metals
	110–120	Yellowish green consolidated muddy silt with faint laminations	12	High Ca; increase of all metals
	120–136	Yellowish green, compacted muddy/silty sand with clumps of mud	<5	Peak of LOI at 130 cm; low Ca, V, Mn, and Fe; slight increase of Rb and Sr
	136–142	Dark green silty, medium grained sand with flat (flaky) dark green/black clasts of silcrete (cf. 5–16); uneven basal contact	13	Peak of Ca, V, Mn, Fe, Sr, and Ba; low S
	142–151	Olive green, compacted silty sand, with clumps of green mud which becomes less compacted toward the bottom	10	High S; low Ca, V, Mn, Fe; high Rb, Sr, and Zr
	151–170	Olive green, compacted silty sand, with clumps of green mud which becomes less compacted toward the bottom	5–12	Rapidly changing geochemical composition (varves)
	170–178		<10	High S; overall low metal concentrations; peaks of Fe and Zn ca. 175 cm
	178–185		20	Low S; high Ca, peak of Ti; low Mn, Fe, Rb, Sr, and Zr
	>185		15	Low concentrations of all metals

TABLE 4 | Summary of the autecological characteristics of the main ostracod taxa identified in the cored successions.

Taxon		Salinity-Conductivity	Permanent/temporary water body	Preferred ionic composition of water; alkalinity	Substrate	Inland habitat
Limnocythere spp. (Figures 15A–D)		Limnetic to lower mesohaline (?), saline-tolerant genus. In the Sua Pan *L. tudoranceai* occurs across a wide salinity range (320 μS cm^{-1} to > 50,000 μS cm^{-1}); it disappears when conductivities exceeded 70,000 μS cm^{-1} [1–5]	Both permanent and temporary; *Limnocythere* species can tolerate seasonal desiccation [1–5]	Enriched in Na+; high alkalinity/Ca ratio. It can tolerate very high levels of chloride. In the Sua Pan *L. tudoranceai* thrives under high concentration of Na+ and $HCO3^-$ [1, 3]	Muddy to sandy [1, 2, 5–6]	Lakes, ponds, swamps [1–6]
Sarscypridopsis	*S. glabrata*	Reported from hyper-saline lakes [5]				Saline lakes, pools [5]
	S. ochracea (Figures 15E,F)		Both permanent and temporary; can tolerate seasonal desiccation [5]		Muddy to sandy; it seems to prefer muddy substrates [5]	Lakes, ponds [5]
Sclerocypris cf. *bicornis* (Figures 15G–I)		Saline [7]	Both permanent and temporary [6–7]	High alkalinity? [6]	Fine-grained substrates [6]	Lakes, pools [6–7]
Ilyocypris spp. (Figure 15J)		Limnetic to oligohaline? Some species of *Ilyocypris* are also found in slightly saline waters [1, 2, 6]	It seems to prefer permanent water conditions [2]	*I. gibba* can tolerate alkalinity up to 25 meq l^{-1} [1]	Muddy to sandy [2]	Pools, ponds, lakes, rivers, and seasonal ditches [2, 6]
Candonopsis spp. (Figures 15K,L)		Limnetic to oligohaline? [2]	Both permanent and temporary [2]	*C. africana* does not tolerate low Ca^{2+} concentrations, high alkalinity, and enrichment in Na+ and Cl^- [1]	Boggy substrate (vegetated?) [2]	Lakes, ponds, swamps [1–2]
Potamocypris spp.		Tolerant to a wide range of conductivity, up to 10^4 μmho/cm [1]; halotolerant freshwater species that disappear above conductivities of 1,500 μS cm^{-1} in the Sua Pan [3]		It does not tolerate low Ca^{2+} concentrations [1]		Lakes, ponds [1–3]

[1] Cohen et al. (1983); [2] Meisch (2000) ; [3] McCulloch et al. (2008); [4] Yin et al. (1999); [5] Martens et al. (1996); [6] Keatings et al. (2010); [7] Bristow et al. (2018).

of 180–250 μm were extracted and prepared according to standard procedures (**Supplementary Material 1**). Equivalent dose (D_e) values were obtained through calibrating the "natural" optical signal acquired during burial, against "regenerated" optical signals obtained by administering known amounts of laboratory dose following the single-aliquot regenerative-dose (SAR) protocol proposed by Murray and Wintle (2000). Dose rate (D_R) was determined by ICP-MS (for the U, Th abundances) and XRF (for K); adjustments were made for water content, and cosmic dose contributions were determined following Prescott and Hutton (1994). Dose rate conversion followed Guérin et al. (2011) and the age was calculated by dividing the D_e by the D_R following procedures in Aitken (1985). All given error terms are computed at one sigma.

RESULTS

Ostracod Fauna

Seven main ostracod taxa were identified in the studied cores (**Table 4**). The most common are: *Limnocythere* species (**Figures 3A–D**), *Sarscypridopsis ochracea* (Sars, 1924; **Figures 3E,F**), and *Sclerocypris* cf. *S. bicornis* (Müller, 1900; **Figures 3G–I**). Other species of *Sarscypridopsis* (mainly *S. glabrata*; Sars, 1924) and valves belonging to genera *Ilyocypris* (**Figure 3J**), *Candonopsis* (**Figures 3K,L**), and *Potamocypris* are also locally recorded. Well-preserved valves of *Limnocythere* species are widely recorded in the dataset, being found at almost all the study sites and throughout the cored successions at different stratigraphic levels. *Limnocythere* spp. commonly

TABLE 5 | Results of the OSL analysis on the samples from the Kubu Island core, including ICP-MS value for Th, U, and K.

Sample ID	Lab ID	Depth	Grain size	Dating material	Dating protocol	Water content	Th	U	K	Dr	OD*	De (CAM)	CAM age	De (MAM)	MAM (Age)
		cm	μm			%	ppm	ppm	(%)	(Gy.ka^{-1})	(%)	(Gy)	(ka)	(Gy)	(ka)
Kubu 20–40	UNB5	30	180–250	Quartz	SRA	16.85	6.57 ± 0.15	1.88 ± 0.03	0.90 ± 0.02	1.78 ± 0.24	62	4.41 ± 0.58	2.48 ± 0.33	2.56 ± 0.43	1.44 ± 0.24
Kubu5 40–60	UNB6	50	180–250	Quartz	SRA	10.47	6.79 ± 0.15	2.20 ± 0.03	1.97 ± 0.02	2.89 ± 0.08	41	83.86 ± 7.79	29.06 ± 2.83	47.85 ± 6.44	16.58 ± 2.28

Other accompanying data are reported in ***Supplementary Material 1****. *Random variations or scatter in the dataset that cannot be explained by the measurement uncertainty are defined as overdispersion (OD) (Galbraith, 1994). The high OD reflects a mixed population in the sample group and therefore indicates incomplete bleaching of some of the grains in the sample.*

FIGURE 3 | Scanning Electron Microscope (SEM) micrographs of ostracod valves from the Makgadikgadi Pan cores. **(A–D)** *Limnocythere* spp. **(E,F)** *Sarscypridopsis ochracea*. **(G–I)** *Sclerocypris* cf. *bicornis*, a close-up view of the muscle scars in **(H)**. **(J)** *Ilyocypris* spp. **(K,L)** *Candonopsis* spp. All scale bars 100 μm.

occurs as the predominant taxa (> 50% of the encountered total valves), locally forming monospecific assemblages. The genus is considered tolerant of waters with a wide range of salinity and alkalinity (**Table 4**). Consistently, *Limnocythere*-dominated assemblages have been frequently reported from littoral, shallow deposits of modern South Africa lakes and wetlands under high salinity and alkalinity levels as well as over wide ranges of Cl^- concentration (Cohen et al., 1983; Martens et al., 1996; Holmes et al., 1998). McCulloch et al. (2008) documented the widespread occurrence of the species *Limnocythere tudoranceai* (Martens, 1990) across the Sua Pan, highlighting its capability to tolerate the wide fluctuating salinities and hydrochemical conditions of

the area also characterized by a high proportion of Na^+ and HCO_3^-.

Sarscypridopsis ochracea is the most common secondary species of the dataset, with a number of valves up to 1/5 of the total assemblage (unique exception one sample where it is the dominant taxa). The genus *Sarscypridopsis* is mostly an Afrotropical genus (Szwarc et al., 2021) and *S. ochracea* is one of the most frequently recorded species in southern Africa within both permanent and temporary water bodies (Martens et al., 1996).

Sclerocypris cf. *S. bicornis* is exclusively recorded from the Ntwetwe Pan with few valves/sample (1–4 valves/sample). The ecology of this species is still poorly known (**Table 4**). Martens (1988) reported a similar species from the Makgadikgadi Pans, *Sclerocypris exserta makarikarensis*, considered as endemic hence perfectly adapted to the seasonal desiccation cycles and the high alkalinity of the water. This seems to be confirmed by Bristow et al. (2018) who found specimens with strong similarity to both *S. bicornis* and *S. exserta* in the sediments of the Lake Megachad (Sars, 1924). These specimens are more quadrate and show a less prominent posterior point compared to *S. exserta*. This "sub-quadrate" shape also typifies the *Sclerocypris* valves found within the cores reported herein (**Figures 3G–I**). *S. bicornis* has also been documented from Lake Turkana and Lake Qarun in Egypt (Keatings et al., 2010), under shallow, saline, permanent water conditions (Keatings et al., 2010). The other encountered ostracods, mainly belonging to genera *Ilyocypris*, *Candonopsis,* and *Potamocypris*, are commonly represented by few valves (a total of less than five valves/sample); these genera seem to be sensitive to high salinity conditions and high levels of alkalinity (**Table 4**).

Morphological observation and SEM-EDS analyses revealed the presence of recrystallized valves and heavily recrystallized carapaces within the majority of the analyzed samples. These ostracod remains retain their overall external shape but are almost entirely silicified, as documented by the EDS intensity spectra that invariably show a marked peak in Si accompanied by a subtle peak in Mg, while the Ca peak appears negligible (**Figure 4**).

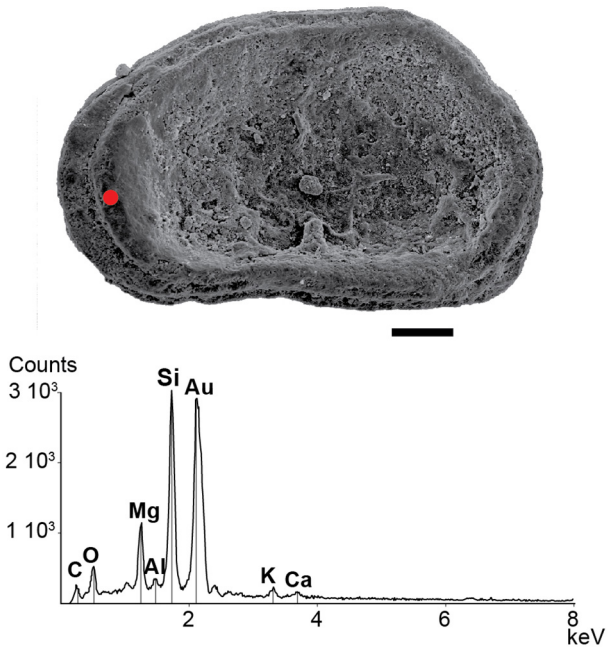

FIGURE 4 | Scanning electron microscope micrograph of a silicified valve of *Limnocythere*. The EDS spectrum shows the Si-bearing composition of the ostracod shell (red spot) found in the core RM3 at 262–265 cm depth (see **Figure 7**). The scale bar is 100 μm.

Sua Pan Cores

Northern Sua Pan

The ∼103 cm long core drilled in the northern portion of the Sua Pan (**Table 1**; point 1 in **Figure 1B**) is detailed in **Table 3** and **Figure 5A**. This core, collected from the pan floor at an elevation of ∼903 m a.s.l., is typified by opposite changes in K and Cl contents, which show a negative correlation (R^2 = 0.75; **Table 2** and **Figure 6A**).

Sediments at depths between 103 and 65 cm consist of sandy silt to very fine, poorly sorted sand, with a greenish, indurated pavement at ∼75 cm depth. These sediments are characterized by high K, Ca, Sr, and Ba contents that decrease upward. The Cl content shows a marked positive peak corresponding to the pavement. A grain size increase is observed between 65 and 38 cm depth, along with an upward decrease of Ca. An opposite trend is observed for K and Cl contents. All major and trace elements, except Cl, show a positive peak at approximately 38 cm depth. Between 38 cm depth and the top of the core, silt to poorly sorted, silty fine sand occurs. K, Ca, and Fe contents decrease upward, while Cl shows an opposite trend.

Kubu Island

A ∼75 cm long core, collected in the vicinity of Kubu Island (**Table 1**; point 2 in **Figure 1B**), is detailed in **Table 3** and **Figure 5B**. This core was collected from the pan floor at an elevation of ∼903 m a.s.l. No evident correlation between the abundances of Cl and K is recorded (**Figure 6B**).

The sediments present at the depth ranging between ∼75 and 55 cm are characterized by dark green silty, fine sand with abundant pebbles, and cobbles of dark green/blackish calcretes and silcretes. The Cl contents exceed those of K; the Ca values are low but increase upcore while Fe shows an opposite trend. Abundant silicified ostracods occur, while well-preserved valves are not encountered.

Between ∼55 and 35 cm depth a normal graded bed made of poorly sorted, fine sand with grains of coarse sand grading into silty, fine sand occurs. This bed is characterized by an overall increase of Fe and other trace elements such as Sr and Ba. Abundant silicified ostracods and rare valves of *Limnocythere* species occur close to the lower boundary of the bed. Upcore, at depth of less than 35 cm, silty fine sands become dominant and an abrupt increase in both the richness and diversity of ostracods occurs. The ostracod fauna includes *Limnocythere* spp. accompanied by *S. ochracea* and species belonging to *Sclerocypris*, *Ilyocypris*, *Candonopsis,* and *Potamocypris* genera.

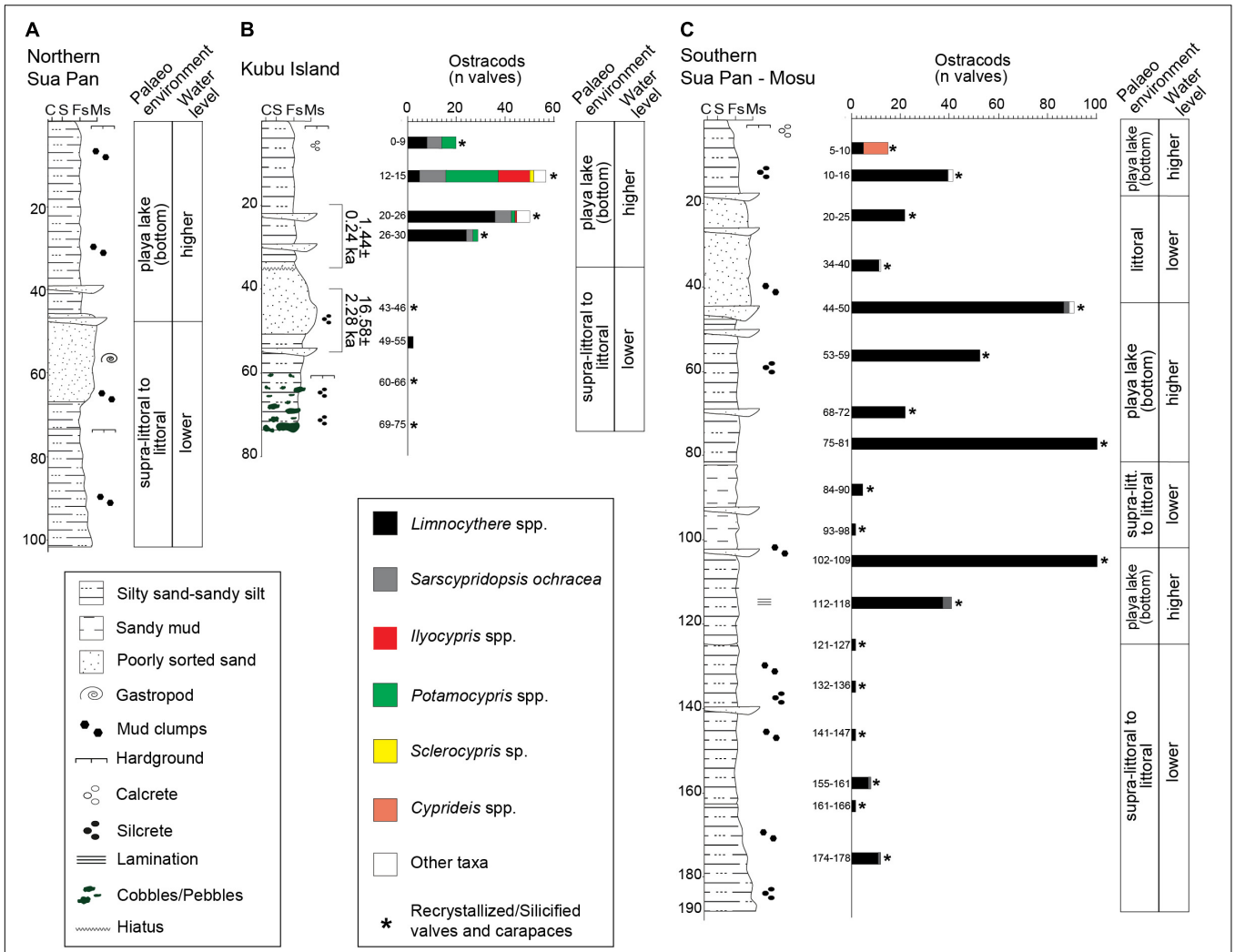

FIGURE 5 | Stratigraphic log, vertical distribution of the main ostracod taxa (reported as number of valves) and palaeoenvironmental reconstruction of the Sua Pan cores. **(A)** Northern Sua Pan. **(B)** Kubu Island. **(C)** Southern Sua Pan-Mosu (see **Table 1** and **Figure 1B** for location).

Southern Sua Pan-Mosu Village

A ∼190 cm long core, collected in the vicinity of Mosu village (**Table 1**; point 3 in **Figure 1B**), is detailed in **Table 3** and **Figure 5C**. This core was collected from the pan floor at an elevation of ∼903 m a.s.l. The sediments at a depth ranging between ∼190 and 125 cm are characterized by olive green, silty sand with mud clumps, and small silcretes. These sediments are typified by opposite changes in K and Cl contents, although no evident correlation is highlighted (**Figure 6C**). The other elements (Ca, Fe, Ba, and Sr) vary every 5 cm or less suggesting laminations, although no visual identification was possible. Ba and Sr elements are slightly more abundant in the bottom portion of the core, in association with coarser sediments. Well-preserved ostracod valves are scarce and mostly represented by *Limnocythere* spp., while silicified ostracods are abundant. Between ∼125 and 100 cm, the dominant lithology is yellowish to light green, very fine, silty sand with interbeds of medium sand. Oscillations in K and Cl contents are broader and the number of ostracod valves, almost exclusively represented by *Limnocythere*, is relatively high.

Between ∼100 and 80 cm depth, light to dark green sandy mud with sand interlayers occur. In this interval, a sharp increase of Cl, Ba, and Sr contents is encountered along with several valves of *Limnocythere* spp. A layer of dark green, fine to very fine, silty sand, observed between ∼80 and 50 cm depth, shows an increase of K, while the Cl content drops together with Ba and Sr, as well as the number of *Limnocythere* valves. Between ∼50 and 20 cm dark green, poorly sorted, fine sand occurs, grading into ∼15 cm of yellowish, medium sand. The Cl content drops while K content is still fluctuating (**Figure 6C**).

The topmost 20 cm of the core comprises greenish, fine, silty sand organized into a fining upward trend. These sediments are characterized by a very low Cl content, and high values of K, Ca, Ba, and Sr. At the top of the core, the ostracod fauna becomes dominated by *Cyprideis* spp. with the second occurrence of *Limnocythere* species.

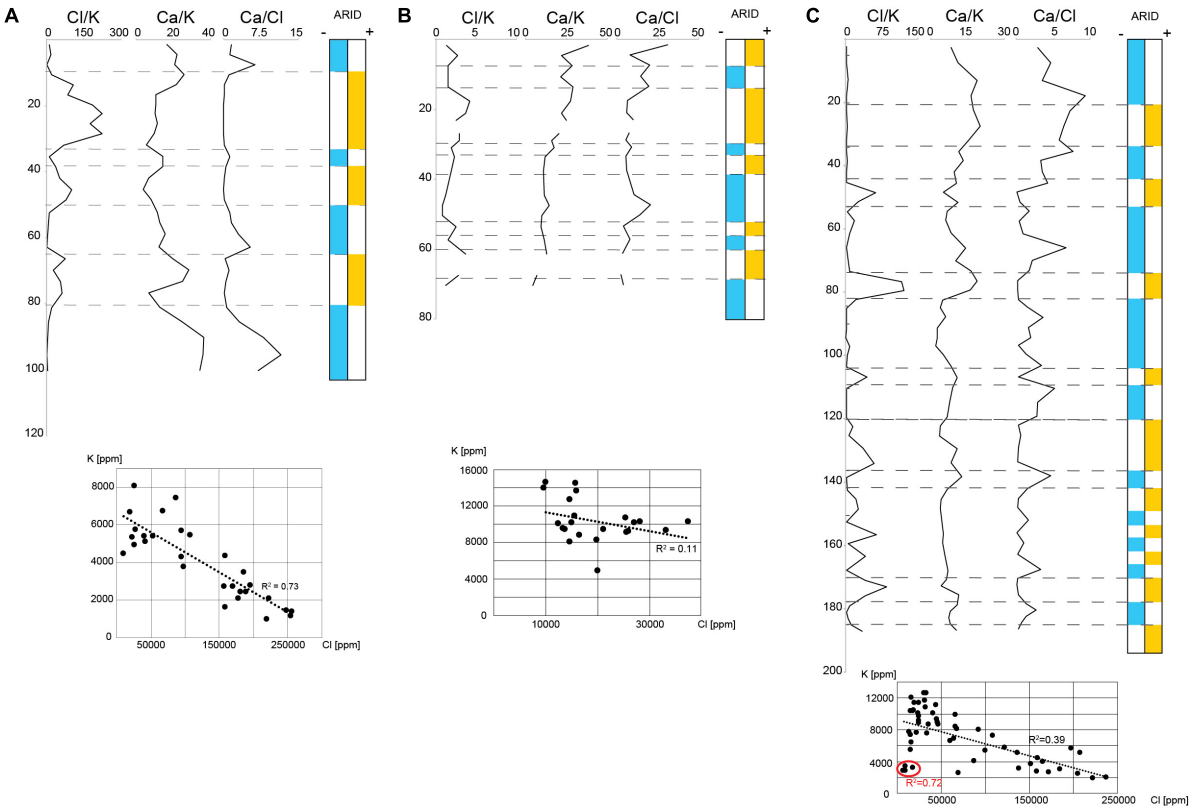

FIGURE 6 | Vertical changes of the Cl, K, and Ca ratios and their interpretation in terms of evaporation rates-dryness in the Northern Sua Pan **(A)**, Kubu Island **(B)**, and Southern Sua Pan-Mosu **(C)**. The cross plots show the degree of correlation between K and Cl.

Ntwetwe Pan Cores

LM Mound

A ∼195 cm long core was drilled along the north-eastern shore of the Ntwetwe Pan at an elevation of ∼919 m a.s.l (point 5 in **Figure 1B**). The sediments found at a depth between ∼195 and 155 cm consist of a fining upward succession of yellowish, poorly sorted fine sand that grades into grayish, fine sand, and silt (**Figure 7A**). Only carapaces of silicified ostracods are found. The sediments become much finer between ∼155 and 70 cm depth with dominant sandy silt and horizons of very dark, consolidated muddy silt. This unit is characterized by several valves of *Sarscypridopsis* species including *S. ochracea*. At a depth between ∼100 and 70 cm, *Limnocythere* spp. becomes dominant with the remarkable occurrence of *Sarcypridopsis*, *Candonopsis,* and *Ilyocypris* species. The topmost 70 cm of the core is made up of light gray, poorly sorted, fine, and silty sand barren of ostracods.

NT Mounds

Two cores were recovered from the top of NT2 and NT3 mounds located in the central northern part of the Ntwetwe Pan at an elevation of ∼916 m a.s.l (**Table 1**; point 4 in **Figure 1B**).

The NT3 core, ∼195 cm in length, is characterized by sandy mud with interbeds of fine sand around ∼180 and 165 cm depth (**Figure 7B**). A faint lamination is observed along with the occurrence of unidentified gastropods and abundant calcretes. Between ∼195 and 180 cm depth, abundant valves of *Limnocythere* with subordinate *S. ochracea* are identified. The number of valves decreases between ∼180 and 155 cm depth. Between ∼155 and 110 cm depth well-sorted, fine, silty sand with faint laminations and abundant calcretes occurs. Except for a small number of valves of *Sclerocypris* cf. *bicornis*, and to a lesser extent *Limnocythere* spp., this interval is barren of well-preserved ostracods but several silicified carapaces are found. The uppermost ∼110 cm of sediments are dominantly poorly sorted, fine silty sand. Fragments of gastropod shells and rare valves of *Limnocythere* spp. and *Sclerocypris* cf. *bicornis* are recorded up to 60 cm; around 70–65 cm an increase in ostracod valves is observed.

The core from mound NT2, ∼135 cm in length, shows a quasi-homogeneous lithology dominated by fine to very-fine, silty sand with abundant calcretes (**Figure 7C**). A layer of olive green, consolidated, muddy sand was identified at ∼135 cm depth where several silicified carapaces of ostracods occur. Between ∼70 and 50 cm, a small number of valves of *Limnocythere* spp., *S. ochracea,* and *Sclerocypris* cf. *bicornis* are found along with numerous silicified carapaces.

Ntwetwe Shore

One core, ∼260 cm long, was recovered from the north-western shoreline of the Ntwetwe Pan (**Table 1**; point 6 in **Figure 1B**).

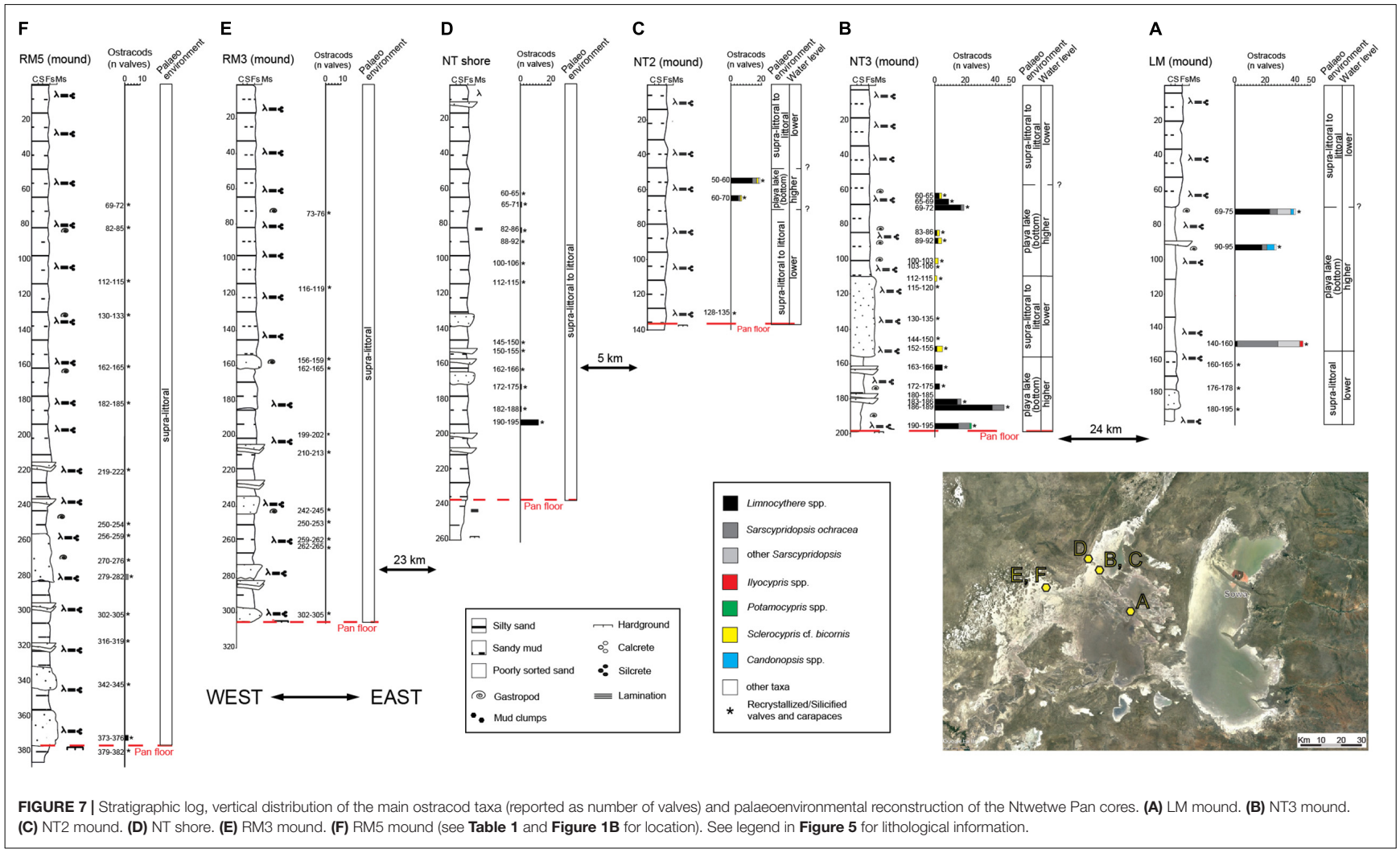

FIGURE 7 | Stratigraphic log, vertical distribution of the main ostracod taxa (reported as number of valves) and palaeoenvironmental reconstruction of the Ntwetwe Pan cores. **(A)** LM mound. **(B)** NT3 mound. **(C)** NT2 mound. **(D)** NT shore. **(E)** RM3 mound. **(F)** RM5 mound (see **Table 1** and **Figure 1B** for location). See legend in **Figure 5** for lithological information.

The bottom corresponds to a pavement of consolidated, silty sand (**Figure 7D**). The sediments between ∼260 and 240 cm are made up of laminated, poorly sorted, silty sand. Between ∼240 and 175 cm depth silty sand with interbeds of medium sand suggest bedding in this portion of the core. Within the uppermost portion of this interval, few *Limnocythere* valves occur accompanied by abundant silicified carapaces. Between ∼175 and 130 cm depth, the sediments are less sorted and the bedding more evident with alternation of poorly sorted, silty sand and sand, exclusively containing carapaces of silicified ostracods. The topmost part of the core is characterized by 130 cm of silty, fine sand containing very few valves of *Limnocythere* and abundant silicified carapaces.

RM Mounds

Two cores, RM3 and RM5 (310 and 390 cm long, respectively), were recovered from the western part of the Ntwetwe Pan (**Table 1**, point 7 in **Figure 1B**).

The RM3 core shows an overall fining upward succession (**Figure 7E**). Between the bottom of the core and ∼120 cm depth, a series of normally graded beds can be distinguished with sparse carapaces of silicified ostracods. These beds grade from fine, silty sand into sandy silt; the basal sands of each graded bed are laminated and feature abundant calcretes and plant remains. The topmost 120 cm of the core is characterized by very fine, silty sand including carapaces of silicified ostracods.

At the bottom, the RM5 core shows a pavement of consolidated silty mud, above which an overall fining upward succession occurs (**Figure 7F**). Between ∼385 and 200 cm depth, a series of normally graded beds have been identified. These beds grade from fine, silty sand to sandy silt; the basal sands of each graded bed are laminated with abundant calcretes and plant remains. Rare valves of *Limnocythere* spp. and *S. ochracea* were found in sandy beds at ∼375 and 280 cm depth, otherwise, only carapaces of silicified ostracods have been identified. The topmost 200 cm of the core are characterized by very fine, silty sand with several carapaces of silicified ostracods.

Optical Stimulated Luminescence Ages

The luminescence ages of the two samples from Kubu Island are reported in **Table 5** and **Supplementary Material 1**. The equivalent dose measurement for all samples recorded a large degree of scattering in the data (**Supplementary Material 1**). The MAM ages obtained from samples Kubu 20–40 cm and Kubu 40–60 cm were 1.44 ± 0.24 ka and 16.58 ± 2.28 ka, respectively.

DISCUSSION

Ostracods were first reported from the sediments of the MB in Grey and Cooke (1977), where a lacustrine environmental context was inferred on the basis of the fauna found along the Gidikwe ridge (**Figure 1A**). Unidentified ostracod valves were also reported from the 20.5–16 ka old deposits of the Mababe Depression (**Figure 1A**), located NW of the MB pans (Shaw, 1985). A saline, lacustrine ostracod fauna including *Limnocythere* species (*L. thomasi*-group and *L.* aff. *inopinata*), *Sarscypridopsis glabrata*, *Potamocypris* aff. *variegata*, and *Ilyocypris* sp. was described from a Holocene terrace on Kubu Island by Riedel et al. (2012, 2014). The novel ostracod dataset, presented in this study, is coupled for the first time with sedimentological, geochemical, and chronological data along the stratigraphic successions recovered from both the Sua and Ntwetwe pans. This bio-sedimentary record provides new insights into the Late Pleistocene–Holocene palaeoenvironmental dynamics of the central Kalahari and the potential relationships with climate variability, as discussed below.

Sua Pan

Bio-Sedimentary Data and Palaeoenvironments

At the southern reaches of the Sua Pan (site 3 in **Figure 1B**), the pervasive fossil record of *Limnocythere*-dominated assemblages across a 190 cm-thick subsurface succession (**Figure 5C**) documents the long-term persistence of shallow, saline lacustrine conditions (i.e., playa lake *sensu* Briere, 2000). The modern distribution patterns of *Limnocythere* species in African wetlands and lakes point to the occurrence of a highly alkaline, chloride-enriched water body, periodically subject to desiccation phases and accompanied by evaporitic conditions (**Table 4** and references herein). Northward, a similar ostracod fauna typifies the 80 cm-thick subsurface succession at Kubu Island (site 2 in **Figure 1B**). Such stratigraphic records extend back into the past the widespread colonization of *Limnocythere* species across the edges of the Sua Pan (McCulloch et al., 2008).

However, the paucity of well-preserved ostracods within the lowermost portion of the Kubu core (∼75–35 cm core depth) and three distinct intervals of the Mosu core ∼190–125 cm, 100–80 cm, and 45–20 cm core depth) reflects the (repeated) establishment of littoral to supra-littoral conditions under the influence of persistently low water levels and intense evaporitic and diagenetic/alteration processes. This interpretation is consistent with an increase of the sandy fraction and the occurrence of silica-rich duricrusts and/or pebbles-cobbles of silcretes, indicative of a playa lake marginal/littoral setting (**Figure 5**). Accordingly, the abundance of silicified ostracods (**Figure 5**), which are invariably predominant with respect to well-preserved valves, suggests the occurrence of strong diagenetic processes in the vadose zone. The recrystallization of ostracod shells can be linked to diagenetic processes driven by acidic, moderately saline conditions in the capillary zone (Ringrose et al., 2005) during periods of subaerial exposure, to which the littoral zone is more exposed. The silicified carapaces are then winnowed by wind erosion, which becomes the dominant geomorphological agent during prolonged low water level phases, and redistributed as aeolian sediments. This would explain why silicified ostracods are almost ubiquitous in the sediments under investigation.

The sandy interval recorded between ∼50 and 35 cm depth at the Kubu Island (**Figure 5B**) is completely barren in well-preserved ostracods and possibly corresponds to a supra-littoral environment mainly affected by wind deflation.

The uppermost part of the Sua Pan cores (∼20 cm in Mosu and ∼35 cm in Kubu) shows a rather abundant ostracod fauna (**Figure 5**) mainly composed of *Limnocythere* spp. and to a

secondary extent of other taxa. Overall, the ostracod richness increases near the Kubu Island site (**Figure 1B**) where valves belonging to *S. ochracea* and genera *Ilyocypris*, *Potamocypris*, *Candonopsis,* and *Sclerocypris* also occur (**Figure 5**). Despite difficulties with ostracod taxonomy and the low degree of knowledge about the autoecology of several species (**Table 4**), this assemblage is interpreted to reflect a lacustrine stage with sustained water availability and low desiccation rates (i.e., high water level), likely accompanied by a slight decrease in salinity and a moderate alkalinity/Ca ratio (**Figure 5B** and **Table 4**).

At the Mosu site, only the uppermost sample (5–10 cm depth) includes an assemblage not dominated by *Limnocythere* that is largely replaced by *Cyprideis* (**Figure 5C**), confirming a recent switch to wetter conditions and an overall drop in alkalinity/Ca ratio (Cohen et al., 1983; Keatings et al., 2010; Wouters, 2017).

Changes in Water Chemistry

Geochemical analyses of sediments from the Sua Pan revealed a clear fluctuation in the relative abundances of Cl, Ca, and K (**Figure 6**). Variability of the Cl/K, as well as Ca/Cl, ratios might suggest changes in the aridity and an increase in the dryness of the basin. Stratigraphic intervals enriched in Ca and depleted in Cl likely reflect wetter conditions characterized by a lower evaporation rate, as chlorides tend to stay in solution for longer due to their higher solubility with respect to Ca-bearing minerals (e.g., calcite). Wetter periods might also record a higher influx of detrital silicates, including clays that lead to an increase in K contents (and further decrease of Cl/K). By contrast, during dryer periods strong evaporitic conditions promote the formation of chlorides over calcite, resulting in an increase of Cl/K paralleled by a decrease in Ca/Cl (**Figure 6**).

Interestingly, the highest peaks of the abundance of *Limnocythere* species in the cores from Kubu (∼20–30 cm depth) and Mosu (∼45, 75, and 100 cm depth) correspond to strong positive peaks in Cl concentration (**Figures 5**, **6**) suggesting a positive relationship between evaporitic conditions and *Limnocythere*-dominated population, consistently with the autoecological characteristics of this opportunistic genus (**Table 4**).

Age of the Sediments at the Kubu Site

The sandy interval found at ∼35–50 cm depth within the Kubu Island core is dominated by silicified ostracods indicating littoral to supra-littoral conditions, chronologically constrained by an OSL-age to 16.58 ± 2.28 ka (**Figure 5B** and **Table 5**). However, the uppermost 35 cm contains the most abundant and rich ostracod fauna of the entire cored succession, pointing to submerged playa lake conditions that, although characterized by high salinity and alkalinity, were slightly more favorable to life than the present-day conditions (**Figure 5B**). This interval, which might represent the last wet phase in the pan, is found to be dating back to 1.44 ± 0.24 ka using the OSL method (**Table 5**). The OSL ages confirm the onset of prolonged dry (lowstand) conditions started around 16 ka ago and continued until ∼2 ka. During the former period, the western edges of the Sua Pan were under constant subaerial conditions with wind erosion and winnowing prevailing over deposition, justifying a potential ∼15 ka hiatus (**Figure 5B**). Afterward, relative environmental stability under wetter conditions took place (Burrough and Thomas, 2013).

Sediments found 3 m deep from a core ∼1.5 km to the north-east of Kubu Island were radiocarbon dated at ∼37 ka cal BP (Riedel et al., 2012, 2014). The overlying sediments at ∼2–1.6 m were dated at ∼4.6–4.4 ka cal BP, whereas sediments between 1.4 and 0.2 m depth yielded ages spanning between 1.8 and 2.2 ka cal BP (Riedel et al., 2012, 2014). The bottom of the core in the Kubu Island (**Figure 5B**) consists of dark sediments (**Table 3**; **Supplementary Material 2B**) that can be correlated with an organic matter-rich layer described between 60 and 80 cm depth by Riedel et al. (2012) (see also Riedel et al., 2014). The authors reported a radiocarbon age of ∼1.8 ka BP for these dark sediments revealing a marked discrepancy between radiocarbon dating and OSL ages (**Table 5**). This might be the result of difficulties in stratigraphic correlations between the two cores and/or lateral variation of depositional environments. However, this discrepancy can also depend on intrinsic problems with radiocarbon dating of organic-rich sediments (Lai et al., 2014; Al-Saqarat et al., 2021) in a playa or playa lake environment, where carbonates are constantly forming and dissolving following complex biogeochemical patterns and pH changes.

Ntwetwe Pan

Bio-Sedimentary Data and Palaeoenvironments

At the northern edge of the Ntwetwe Pan, the bio-sedimentary record of the mound sites (point 4 in **Figure 1B**) documents the succession of palaeoenvironmental changes linked to water level oscillations. At the NT3 mound, the lowermost muddy interval containing a well-preserved ostracod fauna, mostly *Limnocythere* spp. and *S. ochracea*, reflects the development of a shallow, playa lake environment (**Figures 7**, **8**); specifically, the predominance of *Limnocythere* valves points to an alkaline, chloride-enriched water body (**Table 4**). Upcore, a marked drop in the number of ostracods is paralleled by the appearance of sandy layers that anticipate the deposition of a ∼40 cm-thick laminated sandy interval, containing numerous silicified valves/carapaces and a few scattered valves of *Limnocythere* spp. and *Sclerocypris* cf. *bicornis* (**Figure 7B**). This sandy interval is interpreted to reflect a shrinking phase of the lake that induced the subaerial exposure of the lacustrine bottom and the development of littoral to supra-littoral zone subject to wind deflation and recrystallization of ostracods. The re-establishment of a submerged environment is testified by the concomitant change in lithology (decrease in the sandy fraction) and ostracod content (increase in well-preserved valves). The co-occurrence of *Limnocythere* spp., *Sclerocypris* cf. *bicornis,* and, locally, *S. ochracea* points to saline, playa lake conditions developed under rising water levels (**Figure 7**). Accordingly, a similar environmental trend is typified by ostracod fauna at the nearby NT2 mound site. On the contrary, persistent littoral to supra littoral conditions occurred at the NT shore site, located ∼6 km to the NW (point 6 in **Figure 1B**), and along the western side of the Ntwetwe Pan in correspondence of the RM mounds (point 7 in **Figure 1B**), as testified by the scarcity of well-preserved ostracods and the abundance of recrystallized valves/carapaces (**Figures 7D–F**).

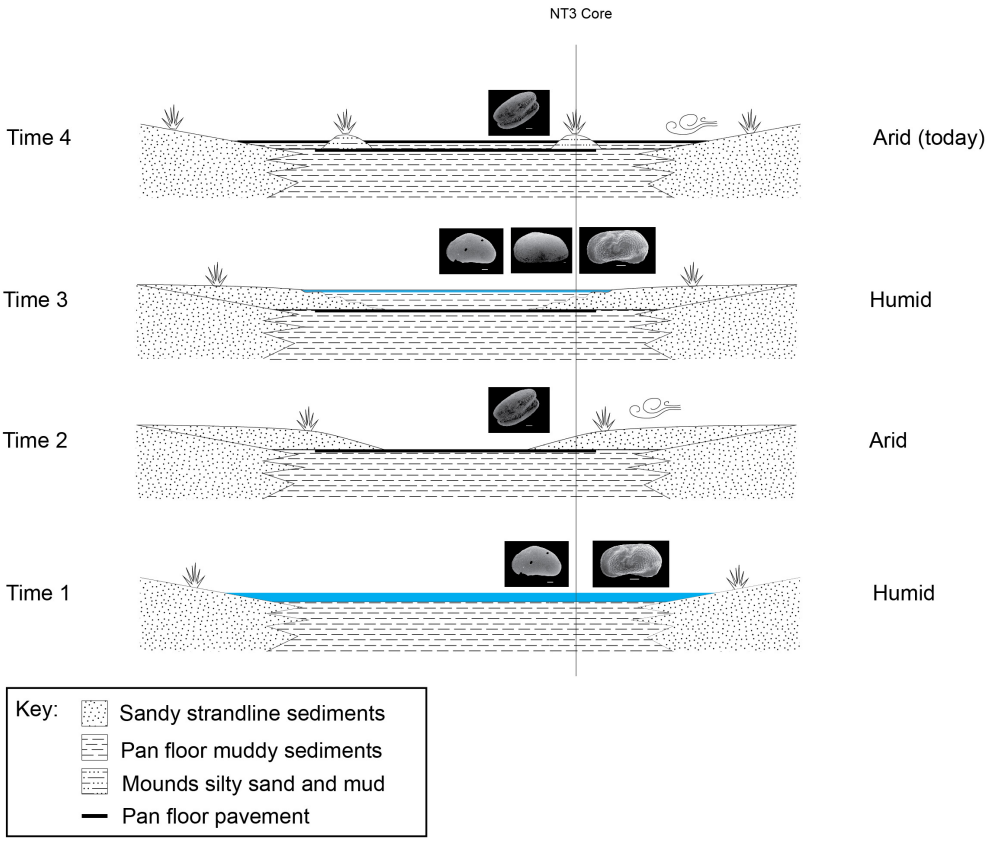

FIGURE 8 | Schematic evolution stages of the LPM since the penultimate highstand phase (17.1 ± 1.6 ka by Burrough et al., 2009a; Schmidt et al., 2017) and the current condition of the ephemeral lake, derived from the cores stratigraphy presented in this study from core NT3 (see **Figure 1B** and **Table 1** for location). The ostracod fauna varies upcore showing a transition from a humid period dominated by *L. inopinata* and *S. ochracea* (Time 1) to a more arid period with abundant carapaces of silicified ostracods and no preserved valve (Time 2). The environment turned toward more humid conditions (Time 3) as shown by the occurrence of *L. inopinata*, *S. ochracea,* and *S. bicornis* at around 80–60 cm depth. Eventually, the environment turned to more arid, playa-like conditions in the recent past (Time 4). Time 1 = ∼17 ka BP; Time 2 = ∼17 ka—2 ka BP; Time 3 = ∼2 ka BP—Medieval Warm Period; Time 4 = Little Ice Age to present day.

Unstable environmental conditions affected the eastern side of the Ntwetwe Pan, as testified by the bio-sedimentary data of the LM mound core (point 5 in **Figure 1B**). The superposition of a ∼1 m-thick muddy interval with a rather abundant and diversified ostracod fauna onto silt-sand deposits exclusively containing recrystallized valves/carapaces reflects an increase in the water level, which led to the submersion of the littoral zone (**Figure 7A**). The relatively high degree of species diversity and the widespread occurrence of *Sarscypridopsis* and *Candonopsis* species likely suggest moderately alkaline waters. The growth of *Limnocythere* spp. likely tracks a shallowing trend culminating with the deposition of littoral silty sands (**Figure 7A**).

The Late Pleistocene–Holocene Palaeoenvironmental Evolution of the Makgadikgadi Basin

The period between 135 and 70 ka was reported as a period of the extreme variability of African climate with megadroughts recorded in large tropical lakes (Malawi and Tanganyika) contraposed to extreme wet conditions in the Kenyan rift valley suggesting high interregional variability (Cohen et al., 2007).

If we consider the radiometric ages provided in literature for the shallow sediments off the shorelines of Kubu Island as reliable, we have to assume that the top 3 m of sediments in the MP are representative of the last 37 ka or less (as the cores presented here are much shorter), although this interpretation can be complicated by the discontinuous stratigraphic record and rapid lateral facies variations. During this time span, four highstand periods were identified at ∼38.7, 26.8, 17.1, and 8.5 ka (Burrough et al., 2009a). At ∼37 ka BP, the level of the water in the MB decreased to 908 m a.s.l. (Riedel et al., 2014). The 3 m-deep, sandy unit dated at 37 ka BP as described by Riedel et al. (2014) deposed into a shallow-water, near-shore environment and is followed by a sedimentary hiatus protracted until ∼4.6–4.4 ka BP. The core presented here (**Figure 5B**) is more proximal to Kubu Island shores (as indicated by the large cobbles and pebbles found at the bottom of the core), hence it records a longer sedimentary hiatus (up to ∼1.4 ka BP) as the area was at a slightly higher elevation and exposed to aeolian erosion under supra-littoral conditions for a longer period during the low stand phase.

The west–east transect in the Ntwetwe Pan shows a clear transition from sandy, littoral environments dominated by *L. inopinata* in the west (**Figures 7D–F**) to circa-littoral and shallow lacustrine environment in the east characterized by higher faunal diversity, especially around 2 m depth and at ∼60 cm from the top of the mounds (**Figures 7A–C**). In summary, the deepest sediments in the Ntwetwe Pan (e.g., core NT3) show high abundances and variability of ostracod fauna corresponding to a phase when the water level was higher than today and conditions allowed different species to survive in the pans. This can represent the last, certain highstand phase (Time 1 in **Figure 8**) at ∼17 ka BP, or point to more recent times when barchan dunes were stabilized into mounds by the onset of wetter conditions (see section "Discussion" in Burrough and Thomas, 2013). The mega-lake phase recorded by Burrough et al. (2009b) at around 17 ka BP was probably induced by the shift of the Inter-Tropical Convergence Zone (ITCZ) and by significantly colder climate with the consequent reduction in evapotranspiration (Riedel et al., 2014). During this phase, the level in the LPM raised as the system was fed by the inflow from the Okwa River. The mouth of the river has been identified south-west of Lake Xau (**Figure 1A**) at an elevation of ∼936–938 m a.s.l. by Riedel et al. (2014). The timeline proposed by Riedel et al. (2014) suggests that the Okwa River ceased flowing at around 17 ka BP. The abrupt end of the Okwa River inflow was allegedly due to the southward movement of the winter rainfall zone (linked to the ITCZ) (Riedel et al., 2014).

After the 17 ka BP high-stand phase, the sediments in the Sua Pan cores record a drop in the water level and a prolonged sediments hiatus likely caused by subaerial exposure under playa conditions (**Figure 5**). The ostracod fauna from the Sua Pan reveals a prolonged desiccation period between ∼17 and 2 ka, probably corresponding to a regional mega-drought (17–8.5 ka reported by Riedel et al., 2014) that dried up the Okwa river and induced a shift to playa conditions similar to those of the present day (see discussion in Richards et al., 2021). Accordingly, the sediments in the Ntwetwe Pan record a protracted arid period during which the size of the inundated part of the pan reduced drastically, and the pan floor was covered by littoral, aeolian deposits (Time 2 in **Figure 8**). This phase is barren of preserved valves and it is instead rich in carapaces of silicified ostracods. According to Burrough et al. (2009a), this prolonged dry period did not lead to a drying out of the LPM, although this seems to be in discordance with what was presented here.

The last highstand phase identified in the literature, i.e., 8.5 ka, corresponds to the height of the African Humid Period in the early to middle Holocene (e.g., Burrough and Thomas, 2013; Bristow et al., 2018). This highstand was not identified in the present study. This might be related to local variations in the physiography of the basin; the samples described by Burrough et al. (2009a) are located almost 100 km away from the sampling sites presented here and close to river mouths. On the other hand, probably the basin during the Holocene was more stable than thought before and similar to the present-day playa lake. This aligns with the recent findings presented in the study by Richards et al. (2021) that describes the place of formation of the fossil dunes (here called mounds) of the Ntwetwe Pan in an environment very much similar to the present-day one, neither drier nor wetter.

The ostracod data presented here show that the top 40 cm of sediments from the Sua Pan show an incredibly abundant and diverse ostracod fauna followed, in the top 10 cm, by sediments barren of ostracods (**Figure 5**). This reflects a rapid shift in the last millennia or two from prolonged dry (Time 2 outlined above) conditions to wetter conditions, then back to a more arid, playa-like environment probably protracted until the present day. During this highstand phase, the Sua Pan was connected to the Ntwetwe Pan (Riedel et al., 2012). This would explain why the Kubu Island ostracod fauna was found at an elevation within the range of the mounds found in the Ntwetwe Pan (**Table 1**). The sediments from the Ntwetwe Pan in fact record a clear return to wetter conditions, after the prolonged dry period, as indicated once again by the higher diversity in the ostracod fauna, with *S. bicornis* and *S. ochracea* occurring together with *L. inopinata* (Time 3 in **Figure 8**). Such a wetter period can be related to the Medieval Warm Period, which is generally linked to overall humid climatic conditions in Southern Africa (Tyson and Lindesay, 1992; Holmgren et al., 1999; Riedel et al., 2012). The Medieval Warm Period might have seen an inflow of water from the south-west, from the Boteti river, feeding the last lacustrine phase of the MB. Evidence for such abundance of water in the Boteti river have been recently discovered in the palaeo-drainage system of the Ntwetwe Pan. Franchi et al. (2020) have described a relict fan delta that is at an elevation comprised between 912 and 908 m a.s.l. (**Figure 1B**) considered the mouth of the palaeo-Boteti River. This coincides with the elevation of the oldest living baobabs on the Kubu Island (∼1 ka) (Riedel et al., 2012, 2014).

The Medieval Warm Period is followed, as already seen in the Sua Pan, by a prolonged dry period that continues to the present day and led to the final desiccation of the playa lake (Time 4 in **Figure 8**). This desiccation phase, probably starting with the onset of the drier Little Ice Age (Tyson and Lindesay, 1992; Holmgren et al., 1999; Riedel et al., 2012), is characterized by a decline in ostracod fauna and dominated by aeolian conditions (Time 4 in **Figure 8**). Nevertheless, this latest stage of evolution is hard to define since the shallowest sediments analyzed from the Sua Pan yielded discordant radiocarbon ages ranging between 1.8 and 2.2 ka cal. BP (Riedel et al., 2014) and OSL age of 1.4 ka (**Table 5**). Other authors suggest that the water level in the Makgadikgadi Basin has dropped below 905 m a.s.l. in the last 100–150 years, responding to a greater aridity spell beginning in the early 19th Century (Giannini et al., 2008; Riedel et al., 2012).

CONCLUSION

Ostracod fauna from the Sua and Ntwetwe pans shows vertical variations across the cores with clear transitions from sediments barren of preserved ostracods and dominated by silicified carapaces, to sediments with a monospecific fauna of *Limnocythere* species, to units with abundant specific diversity where *Limnocythere* ssp., *Sarcypridopsis* spp. (*S. ochracea and S. glabrata*), *Candonopsis* spp., and *Ilyocypris* spp., are found.

Limnocythere is tolerant to a wide range of environmental conditions and seems to prefer shallow waters and very high levels of chlorine in the water. Therefore, a fauna dominated by *Limnocythere* species can be indicative of a playa lake environment, characterized by very shallow water conditions whereby high evaporation and partial desiccation induce strong environmental stress limiting other taxa.

Sediments of the Makgadikgadi Pans record an overall desiccation trend starting with the highstand at ∼17 ka BP. The lowermost sediments present a fauna dominated by *Limnocythere* ssp. and *S. ochracea* indicative of an environment much wetter than the present-day pans. Between 17 and 2 ka BP, the ostracod fauna records prolonged periods of extreme stressful, littoral conditions dominated by *Limnocythere* and periods of contraction of the pan surface characterized by subaerial exposure, with consequent recrystallization of the ostracod carapaces. This prolonged dry spell is followed, at around 1.4 ka BP, by a relative increase in the lake water level under conditions wetter than the present-day and characterized by an abrupt increase of species variability in the pan sediments. This wet phase was observed to continue well into the Medieval Warm Period, after which a prolonged dry period began during the Little Ice Age and continues to the present day, which has led to the final desiccation of the lake and the onset of playa conditions.

Available data reveal a general trend of greater aridity in the Holocene of the central Kalahari and identify a prolonged dry period between 17 and 2 ka BP. This approach and the study of the cores of shallow sediments have high potential to finally unravel the geological history of the Makgadikgadi Basin. Deeper cores from across the pan will enable this reconstruction to be extended further back in time to provide a comprehensive model of the evolution of the LPM.

DATA AVAILABILITY STATEMENT

The raw data supporting the conclusions of this article will be made available by the authors, without undue reservation.

AUTHOR CONTRIBUTIONS

FF and VR conceptualized the work. FF, BC, SF, RM, PM, and AP carried out the field campaign and collected the cores. PM, GM, and VR performed the ostracod analysis. RM and PM performed the sedimentological characterization of the cores. ME performed the OSL dating. FF prepared the tables and figures for the final draft of the manuscript. All authors contributed to the final draft of the manuscript and approved the submitted manuscript.

FUNDING

This research was carried under research permit CMLWS 1/17/4 II (28), granted to FF, by the Ministry of Land Management, Water and Sanitation Services. The field work was partially funded by an IAS Postdoctoral Research Grant (FF) and Europlanet 2024 RI. Europlanet 2024 RI has received funding from the European Union's Horizon 2020 Research and Innovation Programme under grant agreement number 871149.

ACKNOWLEDGMENTS

We would like to thank Omogolo Keobokile and Lefoko Ramakgala (BIUST) for their assistance in the field. We are also grateful to Stefano Claudio Vaiani and Giulia Barbieri for helpful discussion, Giorgio Gasparotto and Maria Roberta Randi for the technical help with the SEM-EDS analysis, and Keyron Hickman-Lewis for proofreading the article.

SUPPLEMENTARY MATERIAL

The Supplementary Material for this article can be found online at: https://www.frontiersin.org/articles/10.3389/fevo.2022.818417/full#supplementary-material

Supplementary Material 1 | Optical Stimulated Luminescence protocol and results.

Supplementary Material 2 | Results of the sedimentary analyses of the cores from the Sua Pan showing core pictures, grain size distribution (Dx10 = 10th percentile; D × 50 = median; D × 90 = 90th percentile), and vertical variations of selected elements (see **Table 2**). **(A)** Northern Sua Pan core; **(B)** Kubu Island core; **(C)** Southern Sua Pan-Mosu core.

Supplementary Material 3 | Results of the sedimentary analyses of the cores from the Ntwetwe Pan showing core pictures and grain size distribution (D × 10 = 10th percentile; D × 50 = median; D × 90 = 90th percentile). **(A)** LM mound. **(B)** NT3 mound. **(C)** NT2 mound. **(D)** NT shore. **(E)** RM3 mound. **(F)** RM5 mound.

REFERENCES

Aitken, M. J. (1985). *Thermoluminescence Dating*. London: Academic Press, 360.

Al-Saqarat, B. S., Abbas, M., Lai, Z., Gong, S., Alkuisi, M. M., Hamad, A. M., et al. (2021). A wetland oasis at wadi gharandal spanning 125–70 ka on the human migration trail in southern jordan. *Quat. Res.* 100, 154–169. doi: 10.1017/qua.2020.82

Amorosi, A., Rossi, V., Scarponi, D., Vaiani, S. C., and Ghosh, A. (2014). Postglacial coastal dynamics, N tuscan coast, italy. *Boreas* 43, 939–954. doi: 10.1111/bor.12077

Bordy, E. M. (2020). Depositional style changes during the permo-carboniferous-early jurassic evolution of the central kalahari karoo sub-basin, botswana. *Geol. J.* 55, 5514–5539. doi: 10.1002/gj.3751

Briere, P. R. (2000). Playa, playa lake, sabkha: proposed definitions for old terms. *J. Arid Environ.* 45, 1–7. doi: 10.1006/jare.2000.0633

Bristow, C. S., Holmes, J. A., Mattey, D., Salzmann, U., and Sloane, H. J. (2018). A late holocene palaeoenvironmental 'snapshot' of the angamma delta, lake megachad at the end of the african humid period. *Quat. Sci. Rev.* 202, 182–196. doi: 10.1016/j.quascirev.2018.04.025

Burrough, S. L., and Thomas, D. S. G. (2013). Central southern africa at the time of the african humid period: a new analysis of holocene palaeoenvironmental and palaeoclimate data. *Quat. Sci. Rev.* 80, 29–46. doi: 10.1016/j.quascirev.2013.08.001

Burrough, S. L., Thomas, D. S. G., and Bailey, R. M. (2009a). Mega-lake in the kalahari: a late pleistocene record of the paleolake makgadikgadi system. *Quat. Sci. Rev.* 28, 1392–1411. doi: 10.1016/j.quascirev.2009.02.007

Burrough, S. L., Thomas, D. S. G., and Singarayer, J. S. (2009b). Late quaternary hydrological dynamics in the middle kalahari: forcing and feedbacks. *Earth Sci. Rev.* 96, 313–326. doi: 10.1016/j.earscirev.2009.07.001

Chan, E. K. F., Timmermann, A., Baldi, B. F., Moore, A. E., Lyons, R. J., Lee, S.-S., et al. (2019). Human origins in a southern african palaeo-wetland and first migrations. *Nature* 575, 185–189. doi: 10.1038/s41586-019-1714-1

Cohen, A. S., Dussinger, R., and Richardson, J. (1983). Lacustrine paleochemical interpretations based on eastern and southern african ostracods. *Palaeogeogr. Palaeoclimatol. Palaeoecol.* 43, 129–151. doi: 10.1016/0031-0182(83)90051-2

Cohen, A. S., Stone, J. R., Beuning, K. R. M., Park, L. E., Reinthal, P. N., Dettman, D., et al. (2007). Ecological consequences of early late pleistocene megadroughts in tropical africa. *PNAS* 104, 16422–16427. doi: 10.1073/pnas.0703873104

Cooke, H. J. (1980). Landform evolution in the context of climatic change and neoto-tectonism in the middle kalahari of north-central botswana. *Trans. Inst. Br. Geogr.* 5, 80–99. doi: 10.2307/622100

Cooke, H. J., and Verstappen, T. H. (1984). The landforms of the western makgadikgadi basin in northern botswana, with a consideration of the chronology of the evolution of lake-paleo makgadikgadi. *Zeitschrift du Geomorphol.* 28, 1–19.

Eckardt, F. D., Bryant, R. G., McCulloch, G., Spiro, B., and Woode, W. W. (2008). The hydrochemistry of a semi-arid pan basin case study: sua pan, makgadikgadi, botswana. *Appl. Geochem.* 23, 1563–1580. doi: 10.1016/j.apgeochem.2007.12.033

Elburg, M., and Goldberg, A. (2000). Age and geochemistry of karoo dolerite dykes from northeast botswana. *J. Afr. Earth Sci.* 31, 539–554. doi: 10.1016/s0899-5362(00)80006-8

Franchi, F., Kelepile, T., Di Capua, A., De Wit, M. C. J., Kemiso, O., Lasarwe, R., et al. (2021). Lithostratigraphy, sedimentary petrography and geochemistry of the upper karoo supergroup in the central kalahari karoo sub-basin, botswana. *J. Afr. Earth Sci.* 173:104025. doi: 10.1016/j.jafrearsci.2020.104025

Franchi, F., MacKay, R., Selepeng, A. M., and Barbieri, R. (2020). Layered mound, inverted channels and polygonal fractures from the makgadikgadi pan (botswana): possible analogues for martian aqueous morphologies. *Planet. Space Sci.* 192:105048. doi: 10.1016/j.pss.2020.105048

Galbraith, R. F. (1994). Some applications of radial plots. *J. Am. Statist. Assoc.* 89, 1232–1242. doi: 10.1080/01621459.1994.10476864

Giannini, A., Biasutti, M., Held, I. M., and Sobel, A. H. (2008). A global perspective on african climate. *Clim. Chan.* 90, 359–383. doi: 10.1007/s10584-008-9396-y

Grey, D. R. C., and Cooke, H. J. (1977). Some problems in the quaternary evolution of the landforms of northern botswana. *Catena* 4, 123–133. doi: 10.1016/0341-8162(77)90014-5

Guérin, G., Mercier, N., and Adamiec, G. (2011). Dose-rate conversion factors: update. *Ancient TL* 29, 5–8.

Haddon, I., and McCarthy, T. (2005). The mesozoic–cenozoic interior sag basins of central africa: the late-cretaceous– cenozoic kalahari and okavango basins. *J. Afr. Earth Sci.* 43, 316–333. doi: 10.1016/j.jafrearsci.2005.07.008

Holmes, J. A., Fothergill, P. A., Street-Perrott, F. A., and Perrott, R. A. (1998). A high-resolution holocene ostracod record from the sahel zone of north-eastern nigeria. *J. Paleolimnol.* 20, 369–380.

Holmgren, K., Karlén, W., Lauritzen, S. E., Lee-Thorp, J. A., Partridge, T. C., Piketh, S., et al. (1999). A 3000-year highresolution stalagmite-based record of palaeoclimate for northeastern south africa. *Holocene* 9, 295–309. doi: 10.1191/095968399672625464

Huntsman-Mapila, P., Ringrose, S., Mackay, A. W., Downey, W. S., Modisi, M., Coetzeed, S. H., et al. (2006). Use of the geochemical and biological sedimentary record in establishing palaeo-environments and climate change in the lake ngami basin, NW Botswana. *Quat. Int.* 148, 51–64. doi: 10.1016/j.quaint.2005.11.029

Joyce, D. A., Lunt, D. H., Bills, R., Turner, G. F., Katongo, C., Duftner, N., et al. (2005). An extant cichlid fish radiation emerged in an extinct pleistocene lake. *Nature* 435, 90–95. doi: 10.1038/nature03489

Keatings, K., Holmes, J., Flower, R., Horne, D., Whittaker, J. E., and Abu-Zied, R. H. (2010). Ostracods and the holocene palaeolimnology of lake qarun, with special reference to past human–environment interactions in the faiyum (Egypt). *Hydrobiologia* 654, 155–176. doi: 10.1007/s10750-010-0379-4

Key, R. M. (1997). "The pre-kalahari geological of the republic of botswana. 1:1,000,000. geophysical information," in *Map Published by Department Geological Survey*, eds D. I. Koosimile and H. Koketso (Lobatse, Botswana).

Kinabo, B. D., Atekwana, E. A., Hogan, J. P., Modisi, M. P., Wheaton, D. D., and Kampunzu, A. B. (2007). Fault system at the southeastern boundary of the okavango rift zone, botswana. *J. Afr. Earth Sci.* 48, 125–136. doi: 10.1016/j.jafrearsci.2007.02.005

Lai, Z., Mischke, S., and Madsen, D. (2014). Paleoenvironmental implications of new OSL dates on the formation of the "shell bar" in the qaidam basin, northeastern qinghai-tibetan plateau. *J. Paleolimnol.* 51, 197–210. doi: 10.1007/s10933-013-9710-1

Martens, K. (1988). Seven new species and two new subspecies of sclerocypris SARS, 1924 from africa, with new records of some other megalocypridinids (crustacea, ostracoda). *Hydrobiologia* 162, 243–273. doi: 10.1007/bf00016672

Martens, K. (1990). Revision of african limnocythere s.s. brady, 1867 (crustacea, ostracoda), with special reference to the rift valley lakes: morphology, taxonomy, evolution and (palaeo) ecology. *Arch. für Hydrobiol. Suppl.* 83, 453–524.

Martens, K., Davies, B. R., Baxter, A. J., and Meadows, M. E. (1996). A contribution to the taxonomy and ecology of the ostracoda (crustacea) from verlorenvlei (western cape, south africa). *South Afr. J. Zool.* 31, 23–36. doi: 10.1080/02541858.1996.11448392

McCulloch, G. M., Irvine, K., Eckardt, F. D., and Bryant, R. (2008). Hydrochemical fluctuations and crustacean community composition in an ephemeral saline lake (sua pan, makgadikgadi botswana). *Hydrobiologia* 596, 31–46. doi: 10.1007/s10750-007-9055-8

McFarlane, M. J., and Eckard, F. D. (2006). Lake deception: a new makgadikgadi palaeolake. *Botswana Notes Records* 38, 195–201.

McFarlane, M. J., and Long, C. W. (2015). Pan flor 'barchan' mounds, ntwetwe pan, makgadikgadi, botswana: their origin and paleoclimatic implications. *Quatern. Int.* 372, 108–119. doi: 10.1016/j.quaint.2014.10.008

Meisch, C. (2000). *Freshwater Ostracoda of Western and Central Europe. Süßwasserfauna Von Mitteleuropa 8/3*. Stuttgart: Gustav Fischer, 522.

Modie, B. N., and Le Hérrissé, A. (2009). Late paleozoic palynomorph assemblages from the karoo supergroup and their potential for biostratigraphic correlation, karoo kalahari basin, botswana. *Br. Geosci.* 84, 337–358. doi: 10.3140/bull.geosci.1122

Modisi, M. P., Atekwana, E. A., Kapunzu, A. B., and Mgwisanyi, T. H. (2000). Rift kinematics during the incipient stages of continental fragmentation: evidence from the nascent okavango rift, northwest botswana. *Geology* 28, 939–942. doi: 10.1130/0091-7613(2000)28<939:rkdtis>2.0.co;2

Moore, A. E., Cotterill, F. P. D., and Eckardt, F. D. (2012). The evolution and ages of makgadikgadi paleolakes: consilient evidence from kalahari drainage evolution. *South Afr. J. Geol.* 115, 385–413. doi: 10.2113/gssajg.115.3.385

Müller, G. W. (1900). Afrikanische ostracoden, gesammelt von o. neumann im jahre 1893. *Zool. Jahrbücher* 13, 259–268. doi: 10.5962/bhl.part.27374

Murray, A. S., and Wintle, A. G. (2000). Luminescence dating of quartz using an improved single-aliquot regenerative-dose protocol. *Radiat. Measure.* 32, 57–73. doi: 10.1016/s1350-4487(99)00253-x

Nash, D. J., and McLaren, S. J. (2003). Kalahari valley calcretes: their nature, origins, and environmental significance. *Quat. Int.* 111, 3–22. doi: 10.1016/s1040-6182(03)00011-9

Nash, D. J., Shaw, P. A., and Thomas, D. S. G. (1994). Duricrust development and valley evolution: process-landform links in the kalahari. *Earth Surface Proc. Land* 19, 299–317. doi: 10.1002/esp.3290190403

Park, L. E., and Cohen, A. S. (2011). Paleoecological response of ostracods to early late pleistocene lake-level changes in lake malawi, east africa. *Palaeogeogr. Palaeoclimatol. Palaeoecol.* 303, 71–80. doi: 10.1016/j.palaeo.2010.02.038

Podgorski, J. E., Green, A. G., Kgotlhang, L., Kinzelbach, W. K. H., Kalscheuer, T., Auken, E., et al. (2013). Paleomegalake and paleo-megafan in southern africa. *Geol.* 41, 1155–1158. doi: 10.1130/g34735.1

Prescott, J. R., and Hutton, J. T. (1994). Cosmic ray contributions to dose-rates for luminescence and ESR dating: large depths and long terms time variations. *Radiat. Meas.* 23, 497–500. doi: 10.1016/1350-4487(94)90086-8

Richards, J., Burrough, S., Wiggs, G., Hills, T., Thomas, D., and Moseki, M. (2021). Uneven surface moisture as a driver of dune formation on ephemeral lake beds under conditions similar to the present day: a model-based assessment from the makgadikgadi basin, northern botswana. *Earth Surface Proc. Land.* 46, 1–18. doi: 10.1002/esp.5215

Riedel, F., Erhardt, S., Chauke, C., Kossler, A., Shemang, E., and Tarasov, R. (2012). Evidence for a permanent lake in sua pan (kalahari, botswana) during the early centuries of the last millennium indicated by distribution of baobab trees (adansonia digitata) on "kubu island". *Quat. Int.* 253, 67–73. doi: 10.1016/j.quaint.2011.02.040

Riedel, F., Henderson, A. C. G., Heußner, K. U., Kaufmann, G., Kossler, A., Leipe, C., et al. (2014). Dynamics of a kalahari long-lived mega-lake system—hydromorphological and limnological changes in the makgadikgadi basin (botswana) during the terminal 50 ka. *Hydrobiologia* 739, 25–53. doi: 10.1007/s10750-013-1647-x

Ringrose, S., Harris, C., Huntsman-Mapila, P., Vink, B. W., Diskins, S., Vanderpost, C., et al. (2009). Origins of strandline duricrusts around the makgadikgadi pans (botswana kalahari) as deduced from their chemical and isotope composition. *Sedim. Geol.* 219, 262–279. doi: 10.1016/j.sedgeo.2009.05.021

Ringrose, S., Huntsman-Mapila, P., Kampunzu, H., Downey, W. D., Coetzee, S., Vink, B., et al. (2005). Sedimentological and geochemical evidence for palaeo-environmental change in the makgadikgadi subbasin, in relation to the MOZ rift depression, botswana. *Palaeogeogr. Palaeoclimatol. Palaeoecol.* 217, 265–287. doi: 10.1016/j.palaeo.2004.11.024

Sars, G. O. (1924). The freshwater entomostraca of the cape province (union of south africa). Ostracoda. *Ann. South Afr. Museum* 20, 105–193.

Schmidt, M., Fuchs, M., Henderson, A. C. G., Kossler, A., Leng, M. J., Mackay, A. W., et al. (2017). Paleolimnological features of a mega-lake phase in the makgadikgadi basin (kalahari, botswana) during marine isotope stage 5 inferred from diatoms. *J. Paleolimnol.* 58, 373–390. doi: 10.1007/s10933-017-9984-9

Shaw, P. A. (1985). Late quaternary landforms and environmental change in northwest botswana: the evidence of lake ngami and the mababe depression. *Trans. Instit. Br. Geogr.* 10, 333–346. doi: 10.2307/622182

Shaw, P. A., Thomas, D. S. G., and Nash, D. J. (1992). Late quaternary fluvial activity in the dry valleys (mekgacha) of the middle and southern kalahari, southern africa. *J. Quat. Sci.* 7, 273–281. doi: 10.1002/jqs.3390070402

Szwarc, A., Martens, K., and Namiotko, T. (2021). Two new cypridopsinae kaufmann, 1900 (crustacea, ostracoda) from southern africa. *ZooKeys* 1076, 83–107. doi: 10.3897/zookeys.1076.76123

Thomas, D. S. G., and Shaw, P. A. (1991). *The Kalahari Environment*. Cambridge: Cambridge University Press, 284.

Tyson, P. D., and Lindesay, J. A. (1992). The climate of the last 2000 years in southern africa. *Holocene* 2, 271–278. doi: 10.1177/095968369200200310

Wouters, K. (2017). On the modern distribution of the euryhaline species Cyprideis torosa (Jones, 1850) (Crustacea, Ostracoda). *J. Micropalaeontol.* 36, 21–30. doi: 10.1144/jmpaleo2015-021

Yin, Y., Geiger, W., and Martens, K. (1999). Effects of genotype and environment on phenotypic variability in limnocythere inopinata (crustacea: ostracoda). *Hydrobiologia* 400, 85–114.

Conflict of Interest: The authors declare that the research was conducted in the absence of any commercial or financial relationships that could be construed as a potential conflict of interest.

Publisher's Note: All claims expressed in this article are solely those of the authors and do not necessarily represent those of their affiliated organizations, or those of the publisher, the editors and the reviewers. Any product that may be evaluated in this article, or claim that may be made by its manufacturer, is not guaranteed or endorsed by the publisher.